AIRBORNE ENERGY GENERATION SYSTEM

_____

A Final Year Project Report

Presented to

SCHOOL OF MECHANICAL & MANUFACTURING ENGINEERING

Department of Mechanical Engineering

NUST

ISLAMABAD, PAKISTAN

_____

In Partial Fulfillment

of the Requirements for the Degree of

Bachelors of Mechanical Engineering

_____

by

Farzan Nabeel

Syed Ammad Sohail

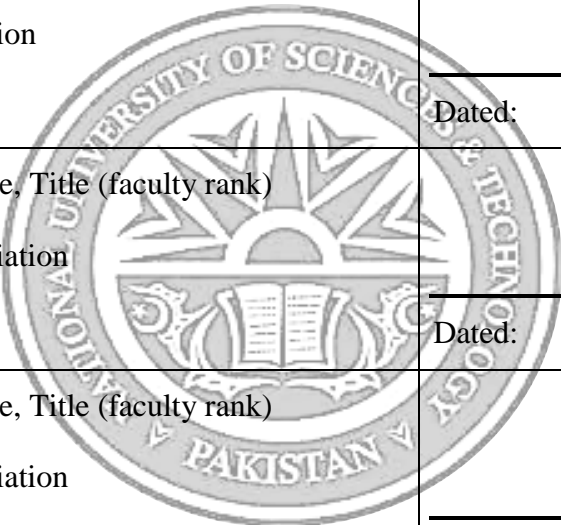Rohail Ahmad Malik

Muhammad Zarrar Mumtaz

June 2022

EXAMINATION COMMITTEE

We hereby recommend that the final year project report prepared under our supervision by:

SYED AMMAD SOHAIL	241554
ROHAIL AHMAD MALIK	270952
FARZAN NABEEL	243588
MUHAMMAD ZARRAR MUMTAZ	245468

Titled: "AIRBORNE ENERGY GENERATION SYSTEM" be accepted in partial fulfillment of the requirements for the award of BACHELOR OF MECHANICAL ENGINEERING degree with grade ___

Supervisor: Dr. Waqas Khalid, Title (faculty rank) Affiliation	 Dated:
Committee Member: Name, Title (faculty rank) Affiliation	 Dated:
Committee Member: Name, Title (faculty rank) Affiliation	 Dated:

_____   _____

(Head of Department)   (Date)

COUNTERSIGNED

Dated: _____   _____

                                           (Dean / Principal

ABSTRACT

An unquestionable fact is; we need more energy. This rhetoric very much implies that we need more energy sources, especially the ones that are clean, green, and renewable.

<u>ACKNOWLEDGMENTS</u>

ORIGINALITY REPORT

TABLE OF CONTENTS

LIST OF TABLES

LIST OF FIGURES

ABBREVIATIONS

CAD	Computer Aided Design
CFD	Computational fluid dynamics
LE	Leading edge
MAC	Mean aerodynamic chord
NACA	National Advisory Committee for Aeronautics
RPM	Revolutions per minute
TE	Trailing edge
Turboprop	Turbo propeller
AWES	Airborne Wind Energy System
AR	Aspect Ratio
AOA	Angle of Attack
HLD	High Lift Device
GPS	Global Positioning System
TR	Taper Ratio
BEC	Battery Eliminator Circuit
BLDC	Brush Less Direct Current
ROC	Rate of Climb
CG	Center of Gravity
PDB	Power Distribution Board
RC	Radio Controlled

NOMENCLATURE

a, A	Aileron
ac	Aerodynamic center
avg	Average
a	Aircraft
b	Baggage
cs	Control surface
cross	Cross-section
C	Crew, ceiling, cruise, cabin
d	Design
D	Drag
e, E	Elevator, equivalent, empty, exit
eff	Effective
E	Engine
f	Fuel, fuselage, flap, friction
GL	Glide
h	Horizontal tail
L	Lift, left, landing
Max	Maximum
Min	Minimum
m	Pitching moment
mg	Main gear
mat	Materials
o	Outboard
opt	Optimum
ot	Overturn
p	Propeller
PL	Payload
r, R	Rudder

R	Rotation
r	Root
ref	Reference
s	Stall, stick
ss	Steady-state
SL	Sea level
TO	Take-off
v, V	Vertical tail
VT	Vertical tail
w, W	Wing, wind
wf	Wing/fuselage

CHAPTER 1: INTRODUCTION

Problem Identification

Wind energy is one of the most prominent and efficient sources of renewable energy. Throughout the world, wind turbines are being used to utilize this energy resource to its fullest potential. However, while these devices are quite efficient and sustainable, they are not without limitations and disadvantages. For instance, wind turbine farms have been found to be prominent sources of noise pollution and produce air turbulence effects which can be detrimental particularly for birds.

They also require significant costs to deploy and produce, most of which goes into the supporting column placing the turbine at some height. This high placement is necessary for the turbine to encounter sufficient wind speeds capable of making the system financially viable. Particularly in Pakistan, this high production and deployment costs is a major reason behind almost complete no exploitation of the technology.

Not only these turbines are costly to deploy, but their supporting columns also need to be highly strong to resist the bending and buckling loads caused by turbulent winds and potential storms. In such cases, the turbines are completely vulnerable to the weather and solely dependent on the strength of support structures. As such, they are also less flexible in deployment and usage.

As can be deduced from the direct relationship between wind speeds and altitude; the higher a turbine is, larger is its power production potential. However, higher turbines would also require sturdier supporting towers to sustain bigger loads, and eventually the structural and manufacturing constraints would result in an unfeasible design. The average level that a windmill lifts the turbine to is around 70-80 meters. In other words, the speedy winds at very high altitudes are unusable by the wind turbines.

To summarize, an alternative is required which:
- Can access high altitude winds (heights ranging from 300 to 1500 meters)
- Is cheaper to produce and deploy (i.e., does not require an expensive and bulky support structure)
- Is more flexible in operation (i.e., easier to undeploy in the event of harmful weather)

- Is sustainable on both collective and individual level (e.g., it can provide sustainable power to small and isolated communities, and produce large amounts of power collectively in wind farms)

Problem Statement

"As per the wind speed's direct correlation with the altitude, a wind turbine must be elevated to increase its power generation potential. However, the structural constraints of the supporting towers eventually limit the maximum reachable height, and even the minimum height requirements make the turbine's production and deployment very costly. So, a more flexible, cheap alternative capable of reaching high altitude winds is needed."

Solution

Over the last few decades, several techniques have been developed by researchers to evaluate methodologies of accessing the high-altitude winds. This data and the thought process surrounding it takes one's attention to potential airborne systems that can be used to harvest energy without using structural bodies to access the high-speed winds.

Such airborne wind energy generation systems are already being utilized around the world, particularly in Northern Europe. These utilize an airborne structure, such as a power kite or a drone, to drive a power production device. They are cheaper, easier to deploy and can easily access high speed winds. Particularly in our case, we converge our attention to three potential systems of this domain: Airborne Kite Power System, Lighter-than-air Power System and Glider Power System.

CHAPTER 2: LITERATURE REVIEW

Airborne Systems' Classification

Airborne Wind Energy Systems (AWES) are typically composed of an airborne unit, such as a power kite, glider, or sailplane, etc., which may or may not be connected to a ground unit via tethers. Such systems may be categorized based on where electricity is generated i.e., on the ground station (Ground-Gen) or the wing (Fly-Gen). To elevate, the object employs updrafts and dynamic soaring in wind gradients. Once in air, the object's profile is manipulated to fly along an optimum path, such as a figure 8 or a circle.

Ground-Gen Systems

A Ground-Gen system generates power at the ground station by transferring the aerodynamic forces from the wing to the ground via tethers, winding and unwinding an electrical generator. These systems normally utilize a pumping cycle, consisting of a generation phase and a recovery phase.

The wind lifts the object to a greater height, creating tension in the tethers and driving the generators. After fully reeling out the tether, the object is flown straight over the ground station allowing the kite to be reeled in at low line tension and thus consuming less energy.

To achieve net positive power generation, the energy created during the generating phase must be greater than the energy utilized during the recovery period. Ground-Gen AWES may be identified in devices with stationary or moving ground stations.

Stationary Ground Station Ground-Gen AWES

Also called Pumping Kite Generators, these systems involve tether coiled on winches attached to the axes of motor-generators. During the generation phase, the airborne object produces a lift force and, therefore, a traction force on the ropes, which drives the generators.
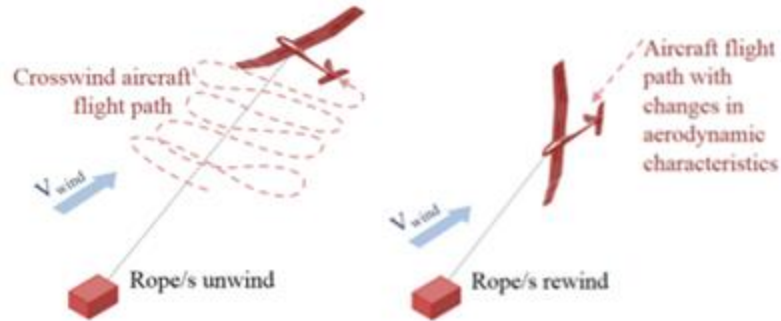
Figure 1: Energy generation (left) & recovery (right) phases of a ground gen system

Crosswind flight, with round or so-called eight-shaped trajectories (yo-yo configuration), is the most employed form of flying during the generating phase. This mode creates a stronger apparent wind on the wing, increasing the traction force exerted on the tether. The motor is responsible for winding back the tethers during the recovery, bringing the wing back to its initial location from the ground.

Generators in Stationary Ground Station Ground-Gen AWES produce a very discontinuous power output with extended alternating time intervals of energy creation and consumption. Because of this, electrical rectification methods must be utilized. Multiple AWES deployed in wind energy farms can greatly minimize the quantity of electrical storage required.

Moving Ground Station Ground-Gen AWES

Moving-ground-station GG-AWES are more sophisticated systems that attempt to provide an always positive power flow to simplify their grid connection. There are many moving ground station Ground Gen AWES designs, but no functioning prototype has been built to yet, and only one prototype is presently under development. Unlike the stationary ground station Ground Gen AWES, the tether winding and unwinding in moving ground station systems does not produce and consume substantial power and is ultimately utilized primarily to regulate the wing trajectory. The generation occurs due to the rotation of the ground station instead of the rope winding mechanism. There are two types of moving-ground-station Ground-Gen AWES:

4

1. *Vertical axis generator*, in which ground stations are attached to the rotor of a massive electric generator with a vertical axis. In this situation, the wing forces cause the ground stations to revolve in tandem with the rotor, transmitting power to the generator.

2. *Rail generators*, which can be either closed loop rail or open loop rail are ground stations that are incorporated on rail cars and create electric energy from vehicle motion. Energy generation in these systems resembles the reverse functioning of an electric train.
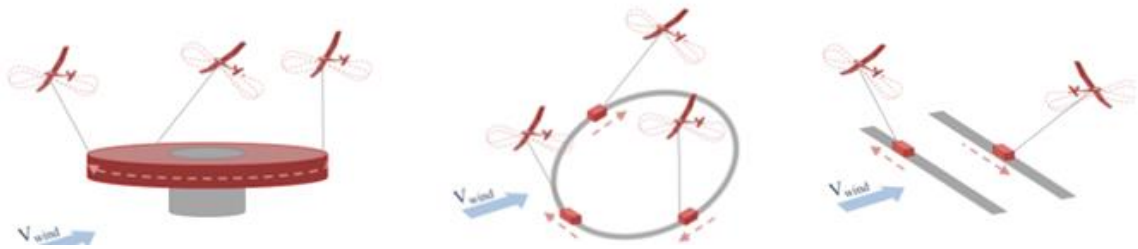
Figure 2: a) Vertical Axis General, b) Close loop rail, and c) Open loop rail

Flying-Gen Systems

Electric energy is generated onboard the aircraft during flight and delivered to the ground through a customized tether that incorporates electric wires. Transformation in Fly-Gen AWES is accomplished using one or more specifically constructed wind turbines/generators. Fly-Gen AWESs may be separated based on their flying principles, which includes *wing lift* (achieved by tethering customized or frames with several wings), *buoyancy and static lift,* which is achieved using aerodynamically designed aerostats loaded with lighter-than-air fluid and *Rotor thrust,* which is achieved using the same turbines/generators that generate electricity.
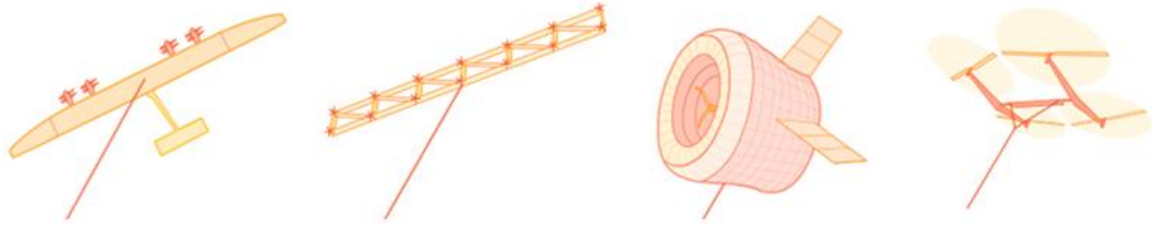
Figure 3: a) Turbines mounted on a glider, b) combination of wing and turbine, c) Aerostat with mounted turbine, and d) Rotor thrust of a quadcopter

Table 1: Different models of Ground-Gen and Fly-Gen AWES

	Type	**Power Rating**	**Altitude**	**Wingspan**	**Generation Mode**
KiteGen KSU-1	LEI-C	40 kW	500 m	20 m^2	Stationary Ground-Gen
KitePower Falcon	LEI-SLE	100 kW	70-400 m	60 m^2	Stationary Ground-Gen
KiteGen ARIA 200	Monolithic Rotor	200 MW	1000m	1 400 000 m^2	Mobile Ground-Gen
Ampyx Power AP3	Glider	150 kW	200-450 m	12 m	Stationary Ground-Gen
Makani M600	Glider with Rotors	600 kW	140-300 m	28 m	Fly-Gen
Sky WindPower Wind Airborne Tethered Turbine System (WATTS)	Autonomous Quadcopter	240 kW	2000m	-	Fly-Gen

Sailplane as an AWES

A sailplane is a heavier-than-air aircraft which solely relies on the natural air currents for altitude gain. As a result, they can soar long distances with a minimum loss of height. Although the words "glider" and "sailplane" are used interchangeably, differences are present between the two based on their aerodynamic performance characteristic. Specifically, sailplanes can provide sustained flight using atmospheric lifting forces and are equipped with a proper fuselage to house passengers or components.

Figure 4: Akaflieg Braunschweig SB-10

Before discussing important features and components of sailplanes, some important concepts relating to their aerodynamics are required to be explained.

Aerodynamics

Figure 5: Forces acting on a cruising sailplane

Lift is the component of the aerodynamic force acting on the plane perpendicular to the direction of airflow. It stems from the differences in air pressure distribution above and below the airplane. Majority of the lift is generated by the wings, which produce a pressure differential above and below them by changing airspeeds on both sides.

Drag is the component of the aerodynamic force acting on the plane parallel to the direction of airflow. Drag can be of two types; friction drag, which is caused by the friction between the object's surface and the flowing air particles, and pressure drag, which is caused by variation of pressure across the body along the flow direction.

The third force acting on a glider in flight is its weight. Weight operates vertically through the glider's center of gravity to counter lift. Because a portion of a glider's weight vector is pointed forwards, gravitational pull also provides some of the force required to propel it through the air.

Thrust is the force that propels the sailplane forward through the air. In self-launching sailplanes, the onboard engine-driven propellors provide this thrust. For unpowered sailplanes, an external force, such as a towplane, winch, or automobile, is used to generate initial thrust. Thrust counteracts drag and maintains speed enough to generate adequate lift which can keep the aircraft airborne. Most sailplanes are designed to produce least amount of drag, so only a high amount of initial thrust is required to keep it airborne.

Maneuverability of a Sailplane

The sailplane can be maneuvered about three axes: vertical, lateral, and longitudinal. All these axes pass through the center of gravity of the sailplane and are mutually perpendicular.
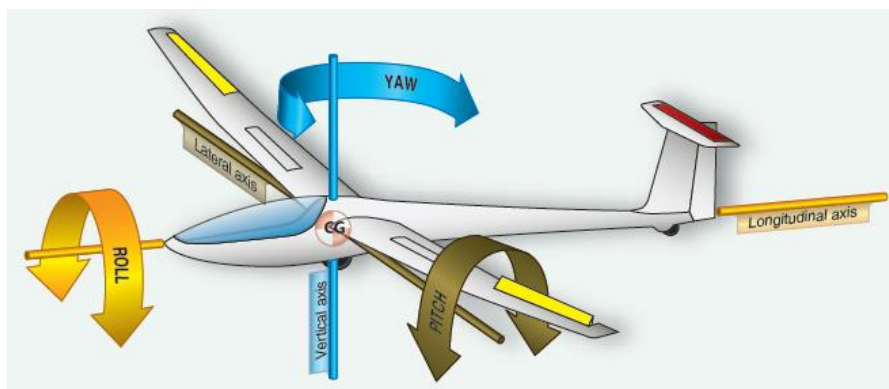
Figure 6: Maneuverability of a sailplane

- The longitudinal axis lies along the length of the fuselage. Movement about the longitudinal axis is called a roll and is controlled using ailerons.

- The lateral axis lies perpendicular to the longitudinal axis. Movement about the lateral axis is called pitching and is controlled using flaps.
- The vertical axis is also perpendicular to the longitudinal axis but is perpendicular to the plane containing the sailplane. Movement about the vertical axis is called yaw and is controlled via rudders.

Glide Ratio and Sink Rate

Glide ratio (also called lift-to-drag ratio) is the ratio between the horizontal distance covered by a sailplane to the corresponding altitude loss. Alternatively, it is the ratio between the lift and drag coefficients at any moment for flight. The glide ratio decreases with speed (since drag varies directly with speed) and increases with the aspect ratio of the wing. The rate at which the sailplane losses its altitude is called its sink rate.

Angle of Attack and Stall

Angle of attack is the angle between the longitudinal axis of the plane and the airflow direction. Both lift and drag coefficients increase when the angle of attack is increased, but only up to a certain value, called the critical AOA. A phenomenon called stall occurs when the AOA exceeds the critical AOA, in which the lift starts to decrease and drag increases drastically. Stall is dangerous for the safe flight and thus avoiding it is one of the design objectives.

Sailplane Components
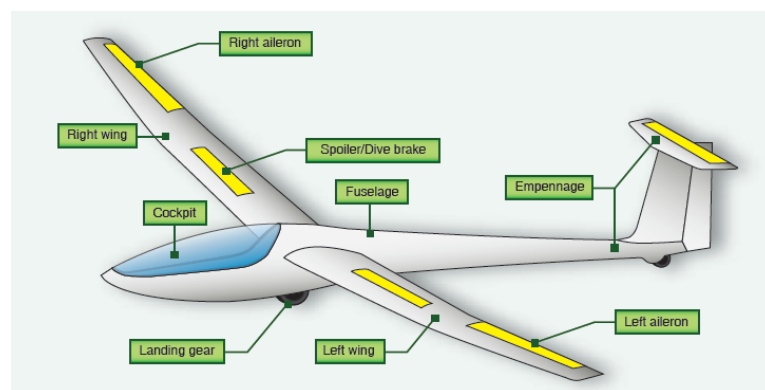
Figure 7: Major Components of a sailplane

Wing

The wing is the most important component of a sailplane since majority of the lift is generated by the wing. Wings have airfoil cross sections, which allows them to produce high amounts of lift while generating low drag and pitching moments. Most sailplane wings have rectangular or trapezoid shapes, although elliptically shaped wings also exist. Important features of aircraft wings in context of sailplane design, are discussed below:

Aspect Ratio

In the context of the sailplane design, the aspect ratio is defined as the ratio of the wingspan to the mean aerodynamic chord. From an aerodynamic point of view, increasing the aspect ratio of the wing makes the non-dimensional aerodynamic coefficients to be closer to the airfoils, since the influence of the wing tip vortices is decreased.

Higher aspect ratios also result in the mass-moment of inertia of the aircraft about its longitudinal axis to increase, which decreases its maneuverability. However, since the sailplanes are generally not designed to be extraordinarily maneuverable, their aspect ratios are quite large, usually in the range 20-50.

Figure 8: ASH 25 (left) with AR = 39.8 & HP-24 (right) with AR = 23.

Incidence Angle

Wing incidence (or wing setting angle) is the angle between wing root chord and fuselage center line. This angle could be constant or could be varied during the flight, although variable incidence angle is usually not recommended due to safety and reliability reasons.

Wing incidence angle always maintains a constant angle of attack between the wing and airflow, and as a result, wing effective angle is increased. Thus, wing can reach stall angle earlier, but also provide higher lift coefficient. Generally, sailplanes do not have an incidence angle as the disadvantages overweigh the advantages.

Taper Ratio

Taper ratio is the ratio between tip chord C_t and the root chord C_r. Essentially, tapering the wing changes the shape of the wing from a quadrilateral to more triangular. Taper ratio varies between 0 and 1, with 0 being a triangular wing and 1 being a rectangular wing. Tapering the wing reduces induced drag on the wing but makes the Reynold's number at the tip lower (due to smaller tip chord), which makes the wing tip stall before root. Earlier stall due to lower effective angle of attack corresponds with higher lift at the tips, resulting into a condition called "tip loading".
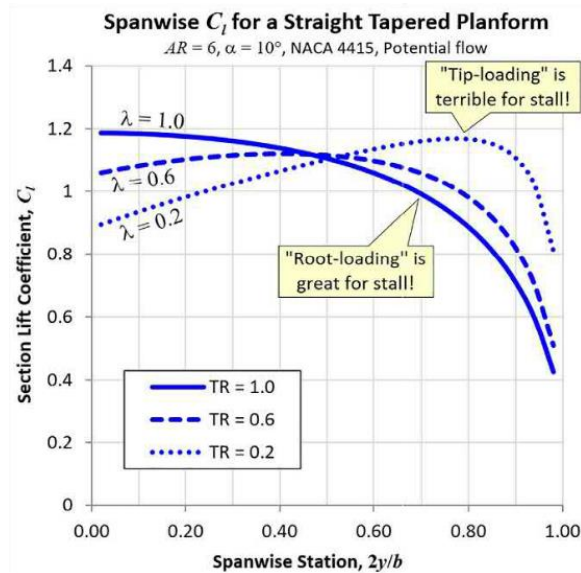
Figure 9: Spanwise lift distribution for different taper ratios

Sweep Angle

Sweep angle is the angle between the edges of the wing and the lateral axis of the aircraft. The edge in question can be the trailing edge (trailing edge sweep) or leading edge (leading edge sweep). The sweep can be forward or backwards, constant or variable.

Using a sweep decreases the effective wingspan along the lateral axis, and as a result improves the lateral controllability of the aircraft since the moment of inertia about the longitudinal axis is decreased.

Wing sweep also decreases the wing lift coefficient and lift coefficient slope and causes the lift loss due to stall at outer portion of the wing to occur behind the aerodynamic center, while the lift ahead of aerodynamic center is maintained. This produces a strong pitching moment and throws the plane into further stall. As a result, swept wings have very poor stall characteristics.

Most of the advantages stemming from the sweep angle only occur at very high speeds, e.g., shockwave drag at transonic speed is decreased via the sweep angle. Since sailplanes move at relatively much slower speeds, very few sailplanes in use have swept wings.

Twist Angle

The difference in the incidence angles of tip and root is called the twist angle. This twist angle maybe positive (tip incidence angle lower than that of root, also called washin) or negative (tip incidence angle greater than that of root washout). Twist angle is used to modify the spanwise lift distribution to be more elliptical or to prevent tip stall before the root. However, this also decreases overall lift coefficient of the wing. Sailplanes generally do not employ twist angles due to cost constraints or because very high aspect ratios already make the distribution elliptical, nullifying the need for a twist angle.

Dihedral Angle

The angle between the wing sections and plane containing the lateral and longitudinal axis is called the dihedral angle. If the wing tip is higher than this plane, the dihedral angle is positive, otherwise it is negative (also called anhedral). For symmetry, both left and right-wing sections must have same dihedral angle. Dihedral angle is used to improve the lateral stability of the aircraft, as the inclined wings produce a restoring rolling moment when the plane is disturbed by a gust. Dihedral angle also reduces the effective wing reference area, which causes a reduction in net lift.

Characteristics of Airfoils
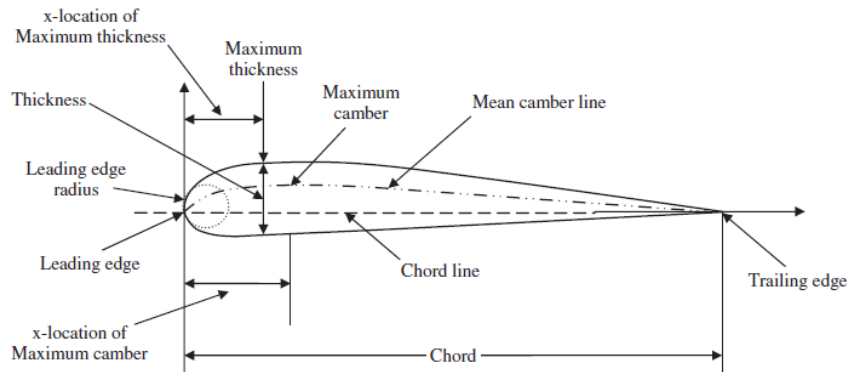
Figure 10: Features of an airfoil

The airfoil shape is responsible for generating the best possible pressure distribution on the wing's top and bottom surfaces so that the desired lift is achieved at the lowest possible aerodynamic expense (i.e., drag and pitching moment). Since sailplanes operate at relatively lower speeds, airfoils specifically designed for low Reynold's number, such as Eppler and Wortmann airfoils are primarily used for sailplane wing design. The length of the airfoil is called its chord.

Many airfoils have a curved profile, which is referred to as camber. Airfoils having higher camber are generally more lift-generating, but also have higher drag coefficients and are difficult to manufacture.

The non-uniform mass distribution about the chord line in certain airfoils results in non-alignment of center of pressure and center of gravity. As a result, the pressure distribution over the airfoil produces a small moment about the center of gravity, which is referred to as pitching moment and is described by a non-dimensional constant called pitching moment coefficient.

The variation of lift, drag and pitching moment with the AOA for an airfoil is studied by its characteristic graphs, which relative non-dimensional lift, drag and pitching moment coefficients, as well as lift-to-drag ratio with the angle of attack.

Important characteristics describing the performance of an airfoil are listed below:

- **Stall AOA:** The AOA at which aerodynamic stall occurs.

- **Zero Lift AOA:** The AOA at which no lift is generated by the airfoil.
- **Maximum Lift Coefficient:** Maximum value of the lift coefficient provided by an airfoil.
- **Ideal Lift Coefficient:** The value of the lift coefficient which does not vary much with the AOA.
- **Zero AOA Lift Coefficient:** The lift coefficient when the AOA is zero.
- **Lift Curve Slope:** The rate of increase of the lift coefficient with the AOA.
- **Stall behavior:** The nature of post-stall lift coefficient loss. This loss maybe abrupt or gentle (more desired as it is recoverable).

Winglet

Winglets are almost vertical extensions of the wings that reduce drag. The difference in air pressure above and below the wing causes tip vortices to form. As a result, generated drag increases and lift at the wingtips decreases. Longer wings or winglets can compensate for the loss of lift while simultaneously reducing generated drag. When employing winglets, the induced drag may be minimized, but the parasitic (form) drag is raised.

Tail
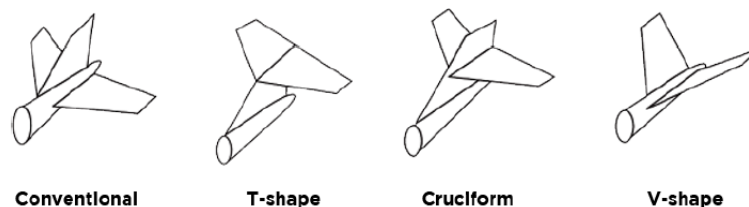
Figure 11: Commonly used tail configurations

The tail's function is to ensure the sailplane's longitudinal and directional stability along longitudinal, lateral, and vertical axes. The horizontal tail provides longitudinal stability, particularly against the pitching moments produced by the wing, while the vertical tail stabilizes the plane along the directional axis.

Some commonly used tail configurations are listed below.

- The conventional tail is the simplest and lightest kind of tail layout. It is made up of a vertical surface and left and right horizontal surface segments.
- The T-tail consists of a vertical surface and a perpendicular horizontal surface positioned on the vertical segment top. It prevents undesirable wing air flows like

14

as wing wake, downwash, and vortices, but can cause a severe stall and is structurally heavier.

- The cruciform is a hybrid of the traditional and T-tail designs. This arrangement includes the upsides and downsides of both types.
- The V-tail configuration comprises of two inclined segments. Since both inclined segments provide force components along both vertical and horizontal axes, a V-tail provides higher stability both longitudinally and laterally but increases drag.

Tails are defined by their efficiencies, which is based upon the flow disruption as air reaches the tail from the wings. The placement and body angles of the tails, such as incidence, twist, and dihedral angles, all perform like those in wings. Horizontal tails are made from symmetric airfoils, which have almost no lift at zero AOA, and thus need to be placed at an incidence angle to generate lift sufficient to balance the pitching moments.

High Lift Device

The concepts of high lift systems are to increase the airfoil camber, increase the wing area, and control the boundary layer by improving pressure distribution, feeding high-energy airflow to the boundary layer, and removing the "old" boundary layer.

A distinction is made between active high lift systems and passive high lift systems. This description is limited to standard passive high lift systems that do not require any additional equipment other than the motor mechanism for retracting and extending the flaps. The high lift devices can be employed at both trailing and leading edges, but here only trailing edge HLDs will be discussed.

- The plain flap is merely a hinged back part of an airfoil, as seen in the diagram. The flap depth of is typically 30 percent of the chord length. By increasing the airfoil camber, the plain flap increases lift. Plain flaps are ailerons, elevators, and rudders.
- Split flaps are no longer utilized since they produce greater drag with the same increase in lift as a normal flap.
- The slot between the wing and the flap gives the slotted flap its name. The specifically formed slit allows air to flow from the bottom to the top of the airfoil. This high-energy flow creates a new boundary layer on the flap's upper surface, allowing flap angles of up to 40 degrees without the flow splitting. As a result, the slot increases maximum lift while lowering drag.
- Fowler flaps have a slot between the wing and flap like slotted flaps.
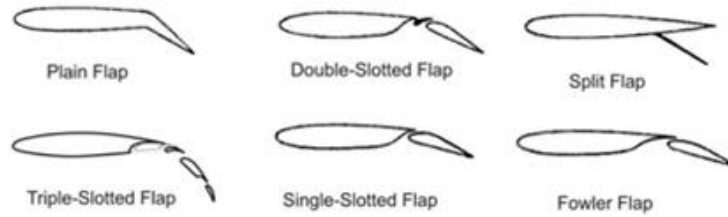
Figure 12: Commonly used HLDs

Flap Kinematics

There are three types of flap kinematics commonly used:

- A dropped hinge mechanism can be used to deflect flaps. The pivot of the flap is located beneath the wing.
- In most cases, if an aerodynamically optimal slot geometry is required for all flap locations, a dropped hinge system cannot be used. A different (complicated) variant provides more options: the flap is mounted on a carriage that moves over a track.
- A linking system is used in a third sort of flap design, which is effectively a compromise between the two forms above.

Instrumentation

Flight instruments in the glider cockpit provide information regarding the glider's direction, altitude, airspeed, and performance. The categories include pitot-static, magnetic, gyroscopic, electrical, electronic, and self-contained. This categorization includes instruments that are sensitive to gravity (G-loading) and centrifugal forces. Instruments can be a basic set used typically in training aircraft or a more advanced set used in the high-performance sailplane for cross-country and competition flying.

Instruments displaying airspeed, altitude, and vertical speed are part of the pitot-static system. Heading instruments display magnetic direction by sensing the earth's magnetic field. Performance instruments, using gyroscopic principles, display the aircraft attitude, heading, and rates of turn. Unique to the glider cockpit is the variometer, which is part of the pitot-static system. Electronic instruments using computer and global positioning system (GPS) technology provide pilots with moving map displays, electronic airspeed

and altitude, air mass conditions, and other functions relative to flight management. Examples of self-contained instruments and indicators that are useful to the pilot include the yaw string, inclinometer, and outside air temperature gauge (OAT).

Flight Control System

The most basic means of directing an airplane is through mechanical or manually operated flight control systems. Pushrods, tension cables, pulleys, counterweights, and sometimes chains are used in a manual flight control system to transmit the forces from actuators to the corresponding components. In scale models, servo motors are used for controlling almost all control surfaces and flaps

Flight Controller

A flight controller is nothing more than a circuit board with electronic chips on it. It is the plane's brain. A little box with smart electronics and software that monitors and controls the operations of the drone. Like the brains of different species, flight controllers vary in size and complexity. These controllers are required for both manual and autonomous flight. For manual flight, the controller needs to be connected to an RC receiver, which connects with a radio transmitter. In case of autonomous flight, the flight controllers utilize information from multiple different sensors, such as GPS, airspeed and gyrometers.

The variation of autonomy in scale models varies from completely autonomous to semi-autonomous planes, which are capable of landing or managing themselves in event of a mishap or communications breakdown and can also stabilize themselves automatically.

Generator

The generator's job is to turn mechanical energy from the turbine shaft into electrical energy that can be stored in the batteries. Voltage, rated current, wattage, and rpm were all important factors to consider while choosing a generator. Because the generator had to be lifted as part of the setup, weight was also a major consideration. Permanent magnet motor generators are a good option since they are dependable and can generate electricity at any rpm.

Storage Accessories

The battery's main function is to transform chemical energy into electrical energy via an electrochemical discharge reaction. The selection of batteries was made based on market research and its parameters. To match the input and output of the generator wattage capacity to store power in the battery and provide variable output, voltage and amperes were the parameters to consider.

Radios, GPS navigation systems, and some flying equipment, such as electric variometers, are all powered by batteries in most gliders. The batteries used are usually Gel batteries, while Lithium-based batteries with higher power and lighter weight have recently become available.

A Lithium Polymer (LiPo) battery is the most reliable choice for sailplane batteries. The current crop of aerial vehicles is conceivable because to the development of the modern Lithium Polymer battery.

CHAPTER 3: METHODOLOGY

Wind Speed and Roughness Factor

To be able to design an efficient and feasible wind energy system, the first step is to bring forth the realization as to what the speed of wind must be. Not all places are suitable for wind energy generation and the selection the place must be based on which place allows for a good wind speed and easy logistical and administrative provisions. This study will begin with the research of where is wind speed high enough for the system to work. To study this efficiently, we begin to access online resources that allow us to find wind data. Our prime focus stays on the twin cities of Islamabad-Rawalpindi since eventually, this system will run within the locality. Later, provisions can be made to allow for this system to be run in other localities as well.

Based on the data from TuTiempo, the average wind speed data from 2010 to 2018 is **12.68 km/h** in Islamabad at ground altitude. Data attained from Global Wind Atlas and Windy suggests that the wind speed currently experienced by Islamabad in November 2021 is around **7.92 km/h (or 2.2 m/s)** at ground.

2010	22.7	30.0	15.9	991.90	13.3
2011	22.3	29.0	15.8	891.81	13.3
2012	22.4	29.0	15.6	909.30	13.8
2013	22.3	28.6	16.2	2557.04	13.4
2014	21.7	28.0	15.8	-	11.2
2015	21.8	27.8	16.2	-	12.7
2016	23.0	29.7	17.1	-	13.3
2017	22.8	29.2	17.1	-	12.7
2018	22.8	29.3	16.7	-	10.5

Figure 13: Air speed at ground over the years (Islamabad)

However, to know what the wind speed will be as we move above, we need to use the Power Law, that employs a parameter called the Roughness Factor. Roughness length is a parameter of some vertical wind profile equations that model the horizontal mean wind speed near the ground. The regions with lower roughness factor correspond to places that have relatively smooth geographical features, allowing the wind to height gradient be

steeper than it would be in places of moderate of high roughness factor. The sea or water bodies naturally have low Roughness factor corresponding to smooth attire of the water body. Based on data from Global Wind Atlas, the regions in Islamabad, near the Rawal Lake falls in Class 1.5 of Roughness length of 0.05 as shown.
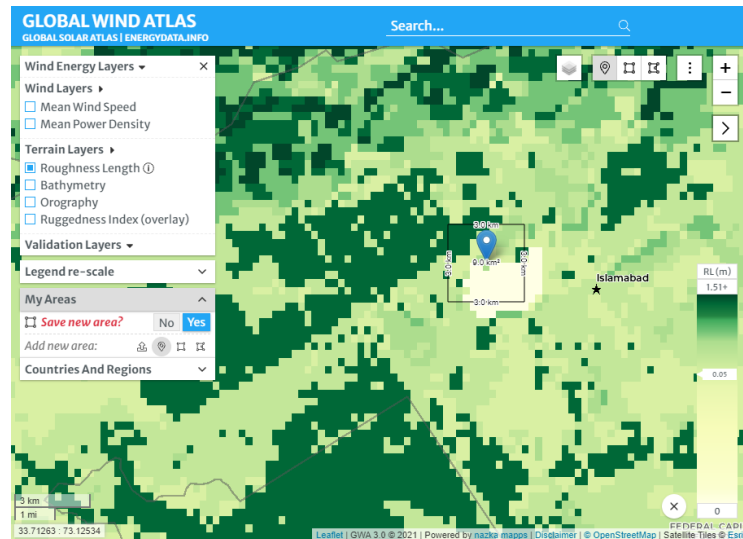
Figure 14: Roughness factor near Rawal Lake

Now we intend to use this roughness factor and the respective equation to map the change in wind speed along the altitude, particularly to find the speed at which the wind blows at the height of around 100 m or 150 m since this is the height that a sail plane is easily capable of acquiring. According to vertical wind profile mapping by Danish Wind Power Association [6], a wind speed of **10 km/h on the ground (as is assumed on a windy day in Rawal Lake Area)**. This means that the wind profile is as shown:
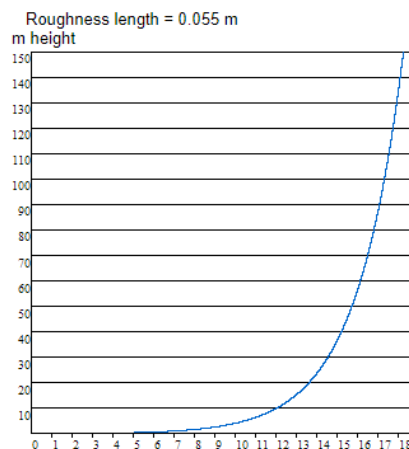
Figure 15: Windspeed variation with altitude at a Roughness factor of 0.055

CALCULATOR							
roughness							
- class	0.0	0.5	1.0	1.5	2.0	3.0	4.0
- length m	0.0002	0.0024	0.03	0.055	0.1	0.4	1.6
150 m	21.86	20.57	18.78	18.25	17.67	16.1	14.09
140 m	21.75	20.44	18.63	18.09	17.5	15.91	13.87
130 m	21.63	20.3	18.46	17.92	17.33	15.71	13.64
120 m	21.5	20.15	18.29	17.73	17.13	15.49	13.39
110 m	21.36	19.99	18.09	17.53	16.92	15.26	13.12
100 m	21.2	19.81	17.88	17.31	16.69	15	12.83
90 m	21.03	19.62	17.65	17.07	16.44	14.71	12.5
80 m	20.84	19.40	17.39	16.8	16.15	14.39	12.14
70 m	20.63	19.15	17.1	16.49	15.83	14.03	11.72
60 m	20.38	18.86	16.76	16.13	15.46	13.61	11.24
50 m	20.08	18.52	16.36	15.71	15.02	13.12	10.68
40 m	19.72	18.11	15.86	15.20	14.48	12.51	9.98
30 m	19.26	17.57	15.23	14.53	13.78	11.73	9.09
20 m	18.6	16.81	14.34	13.6	12.8	10.63	7.83
10 m	17.48	15.52	12.81	12	11.13	8.74	5.68
	Plot	Plot	Plot	Plot	Plot	Plot	Plot

Figure 16: Wind speeds at different altitudes with different roughness lengths

As the data suggests, wind speed as high as **18km/h** can be attained at a height of **150 m** above the ground level on a good day with **12km/h** wind speed on **ground**, near Rawal Lake. This also suggests that a speed of **17.31 km/h** is available on **100 m** height.

On Board Generator Specifics
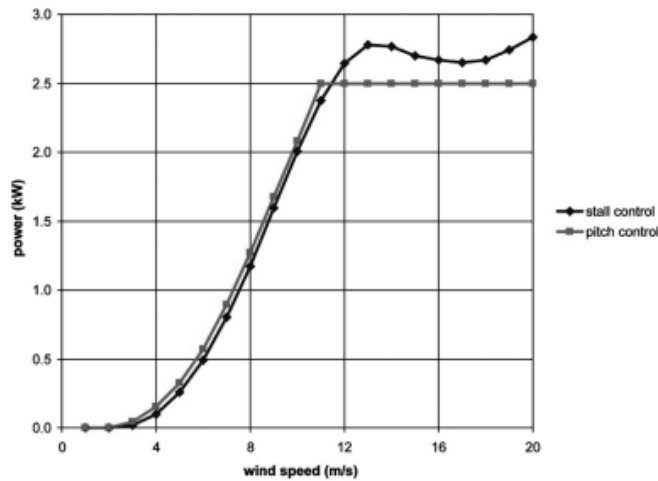
Figure 17: Power and Speed of wind relation

Currently three-bladed wind turbines with horizontal-axis dominate the market. To ensure the wind turbine is always producing the maximal amount of electric energy, the

yaw drive is used to keep the rotor facing into the wind as the wind direction changes. Active stall control means that the turbine will actively change the shape of the blade to begin slowing the rotor when wind speeds reach a certain level. Tip brakes, or speed brakes can deploy mechanically on the blades when the turbine reaches a certain speed.

Pitch control, on the other hand, uses a system that instructs each individual blade to rotate from power to feathered position. It's an active, mechanical process. It should be noted that it is difficult to get the same high aerodynamic efficiency on small turbines as on large turbines. This has to do with the formation of turbulent boundary layer on the surface of the blade. Towards the leading edge of the blade the boundary layer is laminar, but at some critical distance l across the blade surface the flow becomes turbulent. This distance is a function of flow velocity (V), Reynolds number (Re), viscosity (m) and density (m) as per the following equation:

$$l = \frac{(Re * \mu)}{V * \rho}$$

This turbulence reduces pressure drag (the primary effect) and increases friction drag (a secondary effect), with the net effect being a reduction in drag and an improvement in rotor efficiency. Small wind turbine blades have a small chord length and therefore there is a relatively smaller region across the blade surface where the flow is turbulent compared to large turbine blades, hence the higher efficiency from large turbine blades.

Traditionally small wind turbines use DC generators. The DC generator is now usually a permanent magnet three-phase synchronous AC generator (alternator), with a diode rectifier either located up in the turbine (with two wires coming down the tower) or at the control panel (with three smaller wires coming down the tower). The rotor mounts directly onto the alternator shaft, and no gearbox is required.

Preliminary estimates of rotor diameter can easily be made using simple actuator disc theory. Several factors need to be considered, i.e., the wind regime in which the turbine is to operate and the tip–speed ratio. Various losses must be allowed for the main ones being the mechanical transmission including gearbox losses and the electrical generation losses. From the actuator disc theory, the turbine aerodynamic power output is:

$$P = \rho A C_P C_{X1}^3$$

Under theoretical ideal conditions, the maximum value of Cp=0.593. According to Eggleston and Stoddard, rotor Cp values as high as 0.45 have been reported. Such high, real values of Cp relate to very precise, smooth airfoil blades and tip–speed ratios above 10. For most machines of good design, a value of Cp from 0.3 to 0.35 would be possible. With a drive train efficiency, ηd, and an electrical generation efficiency, ηg, the output electrical power would be:

$$P = \rho A C_P \, \eta_G \, \eta_D C_{X1}^3$$

At p =1.166 kg/m^3, C$_p$ = 0.3, η$_g$ & η$_d$ as 0.75 and 0.85 respectively. At approximately 15 m/s speed; the area of the propeller fan shell is approximately 0.133m^2. This gives a 0.2058 m or 20 cm length single blade which is the required blade length in a three-blade propeller.

Cruise Parameters

After determining the wind speed and corresponding energy availability, we now move on to the initial parameters that need to be determined for the analysis of the wing of our glider. There are primarily three important parameters that we need to determine for us to be able to move ahead with calculations about the wing area and the hence the lift and drag study. The very first is the determination of height at which our aircraft will cruise.

Cruise Height

Considering that we have a wind speed of approximately 4m/s available at the height of 100m above the surface, we set the ideal threshold of cruise of plane at 100m above the ground. This being our analytic study, a height of beyond this will correspond to higher wind speed and will therefore allow us to be conservative with our analysis.

Density at Cruise Height

Considering that density of air decreases with altitude, an online tool is used to acquire exact density at cruise height. The Air Pressure and temperature along with the due point is acquired based on Islamabad's data. The solution comes out to be 1.16507 kg/m^3 at the height of 100 m.

Figure 18: Air Density at 100m

Preliminary analysis

An airplane is designed in three phases, according to the systems engineering approach: conceptual design, preliminary design, and detailed design. The airplane will be designed in concept without precise calculations during the conceptual design phase. To put it another way, practically all the parameters are set using a decision-making and selection technique. The results of a mathematical technique, on the other hand, are frequently used in the preliminary design phase.

Aircraft maximum take-off weight (WTO), wing reference area (S), and engine thrust, or power are three key aircraft parameters calculated during the preliminary design phase. Different design requirements, such as stall speed, maximum speed, etc., are laid out, and each of these variables is placed into an equation which gives engine power and wing area per unit weight (power and wing loading, W/P and W/S). All these equations can then be solved by plotting their graphs to generate the optimum design point in terms of wing and power loading.

Maximum takeoff weight is also a design requirement, and thus needs to be laid out before determining the wing and power loading. It can then be multiplied by the said loading values to obtain the exact wing area and engine power.

Maximum Take-off Weight

The sailplane's maximum takeoff weight is set at 7.5 kg. Since it is to be made from lightweight materials and is a scale model, a 7.5 kg weight is more than what will really be its weight and will allow it to lift bigger generators if more power output is required.

Maximum Speed

The maximum speed of the sailplane can be approximated using the available motors used for thrusting provision. Usually, brushless DC motors are used in scale plane models. Since the sailplane generates adequate amounts of lift to keep afloat, the maximum thrust required is quite low compared to the maximum takeoff weight. Since the maximum takeoff weight is 7.5 kg, a thrust capable of moving a 5 kg weight is more than sufficient for the sailplane. The sailplane is to be powered by two similar motors mounted below the wings, so each motor must provide a maximum thrust of 2.5 kg.

From the catalogues of available brushless DC motors, Dongxingwei C3542 motor can provide the required thrust, and thus is chosen as the thrust source for the sailplane. Observing that the maximum power of each motor is around 533 W, and using the fact that power is the product of force and velocity, while assuming a motor efficiency of 70% gives the maximum plane speed of 22 m/s.

The equation relating the wing and power loading to the maximum speed V_{max} is given as follows:

$$\left(\frac{W}{P_{SL}}\right)_{V_{max}} = \frac{\eta_P}{\frac{1}{2}\rho_o V_{max}^3 C_{D_o} \frac{1}{\left(\frac{W}{S}\right)} + \frac{2K}{\rho\sigma V_{max}}\left(\frac{W}{S}\right)}$$

Stall Speed

Stall is the minimum speed that the glider must achieve under all circumstances to maintain its glide trajectory. At any speed below stall, the glider would take a nose-down trajectory towards the ground. The value must be kept such that as soon as the speed of the glider approaches the stall, the motor starts to increase the speed back to cruise speed for the trajectory to be maintained.

The stall speed is selected to be 8.5 m/s based on the data of existing sail planes. The equation relating the wing and power loading to the stall speed V_s is given as follows:

$$\left(\frac{W}{S}\right)_{V_s} = \frac{1}{2}\rho V_s^2 C_{L_{max}}$$

Take-off Run

Another important factor in aircraft performance is the take-off run (S_{TO}), which is the distance between the take-off starting point and the position of a conventional obstacle that the aircraft must clear. Because every airport has a restricted runway, take-off requirements are typically stated in terms of minimum ground run requirements. Taking in consideration realistic situations, the takeoff run for the plane is set at 20 meters.

The takeoff speed is usually 10 to 30 percent higher than the stall speed, and the equation relating the wing and power loading to the takeoff run S_{TO} is given as follows:

$$\left(\frac{W}{P}\right)_{S_{TO}} = \frac{1 - \exp\left(0.6\rho g C_{D_G} S_{TO}\frac{1}{W/S}\right)}{\mu - \left(\mu + \frac{C_{D_G}}{C_{L_R}}\right)\left[\exp\left(0.6\rho g C_{D_G} S_{TO}\frac{1}{W/S}\right)\right]}\frac{\eta_P}{V_{TO}}$$

Rate of Climb

The rate of climb is defined as the aircraft speed in the vertical axis or the vertical component of the aircraft airspeed. Hence, ROC is about how fast an aircraft gains height.

Following equation relates wing and power loading to the rate of climb. The propellor efficiency is assumed to be 55 percent for a conservative estimate:

$$\left(\frac{W}{P}\right)_{ROC} = \frac{1}{\frac{ROC}{\eta_P} + \sqrt{\frac{2}{\rho\sqrt{\frac{3C_{D_o}}{K}}}\left(\frac{W}{S}\right)}\left(\frac{1.155}{(L/D)_{max}\,\eta_P}\right)}$$

Absolute Ceiling

The absolute ceiling, as the name implies, is the highest altitude at which an aircraft can maintain level flight. The ceiling, in other words, is the altitude at which the ROC is zero. Given the operational height of 100 meters, the absolute ceiling for the sailplane is set at 150 meters. Following equation relates wing and power loading to the absolute ceiling:

$$\left(\frac{W}{P_{SL}}\right)_{AC} = \frac{\sigma_{AC}}{\sqrt{\rho_{AC}\sqrt{\frac{3C_{D_o}}{K}}}\left(\frac{W}{S}\right)\left(\frac{1.155}{(L/D)_{max}\,\eta_P}\right)}$$

Wing and Power Loading Estimation

Inserting the set design requirements, and certain assumptions of various coefficients based on the available data from experiments and already existing relevant plane models, the following graph can be obtained by plotting the above-mentioned equations:
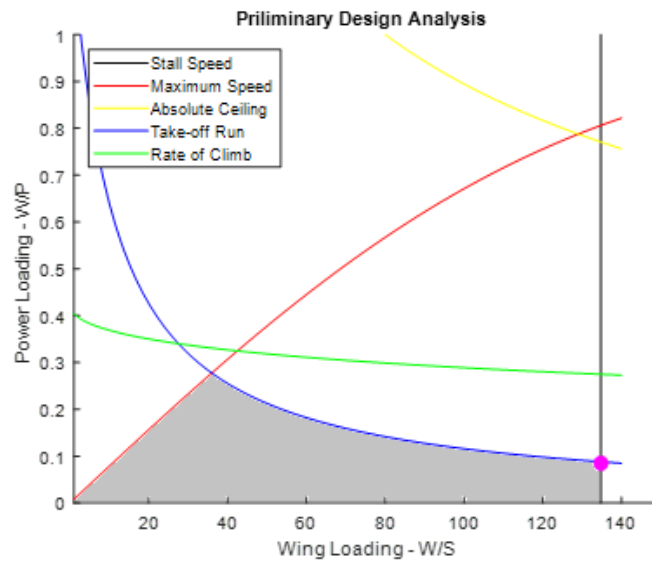
Figure 19: Preliminary Analysis

As the sailplane is designed to consume minimal energy while cruising, the power loading is not a very concerning parameter since it incorporates the maximum power required, which is only during takeoff.

Therefore, to minimize the plane area, the design point (pink dot) is chosen to be at extreme right of the optimum region (the highlighted bottom of the graph) which gives the values of power and wing loading at 0.13 N/W and 100 N/m^2. For a sailplane with maximum take off weight of 7.5 kg, this gives a maximum required power (mechanical) of 577 W and a wing area of 0.75 m^2.

Based on the available data from existing models, the wingspan is selected to be 3 meters, to make the scale model a bit smaller and more adaptable. The wing area of 0.75 m^2 and a span of 3.5 meters give a Mean Aerodynamic chord of around 24.2 centimeters.

Final Parameters

Based on this study, the final parameters are:

- Aircraft General
    - Wing Loading = W/S = 100 N/m^2
    - Power Loading = W/P = 0.13 N/W
    - Maximum Weightlifting Capacity = W_{TO} = 75 N = 7.6 kg
    - Wing Reference Area = S = 0.75 m^2
    - Mechanical Power Consumption = P = 576.92 W
    - Electrical Power Consumption (assuming 60% efficiency) = 950 W
- Speeds
    - Plane Stall Speed = V_s = 8.615 m/s
    - Plane Max. Speed = V_{max} = 22 m/s
    - Plane Cruise Speed = V_{cr} = 1.5*V_s = 13 m/s
    - Wind speed @ 100 m = ~ 4.5 m/s (to be on the safe side assuming ~3 m/s)
    - Plane Cruise Speed relative to the wind = V_c = 13 + 3 = 16 m/s
- Air
    - Air Density at Ground = p_o = 1.225 kg/m^3
    - Air Density at Cruise Altitude = p = 1.160 kg/m^3
    - Air Viscosity = μ = 1.8 x 10^-5 Pa

Airfoil Selection

The characteristics graphs of the airfoil vary with the flow Reynold's number. Therefore, Reynold's number at the cruise speed first needs to be determined. At the operational height of 100 m, with a mean aerodynamic chord length of 24.2 cm and a relative wind speed of 16 m/s, the flow Reynold's number during cruise comes out to be:

$$Re = \frac{\rho V l}{\mu} \approx 250\ 000$$

Based on the sailplane parameters, the desired values of lift coefficients are calculated as follows:

Table 2: Desired Lift Coefficients for the airfoil

Aircraft Ideal Cruise Lift Coefficient	$C_{L_C} = \dfrac{2W_{ave}}{\rho V_c^2 S}$	0.6735
Wing Cruise Lift Coefficient	$C_{L_{C_w}} = \dfrac{C_{L_C}}{0.95}$	0.7089
Airfoil Ideal Lift Coefficient	$C_{l_i} = \dfrac{C_{L_{C_w}}}{0.9}$	**0.7877 ~ 0.77**
Aircraft Maximum Lift Coefficient	$C_{L_{max}} = \dfrac{2W_{TO}}{\rho_o V_s^2 S}$	2.1998
Wing Maximum Lift Coefficient	$C_{L_{max\_w}} = \dfrac{C_{L_{max}}}{0.95}$	2.3156
Airfoil Gross Maximum Coefficient	$C_{l_{max\_gross}} = \dfrac{C_{L_{max\_w}}}{0.9}$	2.5729
HLD Maximum Lift Coefficient	$\Delta C_{l_{HLD}}$	0.8 (assumed)
Airfoil Net Maximum Coefficient	$C_{l_{max}} = C_{l_{max\_gross}} - \Delta C_{l_{HLD}}$	**1.7729 ~ 1.78**

The calculations result in required ideal and maximum lift coefficients to be approximately 0.77 and 1.78, respectively. From the experimental low-speed airfoil data published by the University of Illinois, following airfoils were selected based on their ideal and maximum lift coefficients. All values at a Reynold's number of 250 000.

Table 3: Selected Airfoils & their characteristics

	CH10-48-13	FX-74CL5140	S1223	FX-63-137B
C_{lmax}	2.00	2.14	2.30	1.72
C_{li}	1.16	1.20	1.02	1.00
C_{dmin}	0.019	0.015	0.018	0.012
C_{lo}	1.159	1.201	1.200	0.908

C_{do}	0.019	0.018	0.018	0.015
C_{mo}	-0.269	-0.250	-0.270	-0.212
$(L/D)_{mx}$	80	95	85	112
α_s (degrees)	11	12	13	12.5
α_{ol} (degrees)	-15	-15	-7	-7
C_l/α (/deg)	0.08	0.09	0.0807	0.1
Stall Quality	Moderate	Sharp	Moderate	Docile

From the above mentioned four airfoils, Wortmann FX-63 137B is selected. While its maximum and zero AOA lift coefficient are not the highest, its lower drag and pitching moment coefficients make it a suitable candidate for a stable and less drag inducive sailplane. Furthermore, it also has the highest lift-to-drag ratio, which is very much desirable for sailplanes as it directly correlates to their sink ratio.

The characteristic graphs of FX-63 137B and its profile are illustrated in the figures below. All graphs provide the values at a Reynold's number of 250 000.
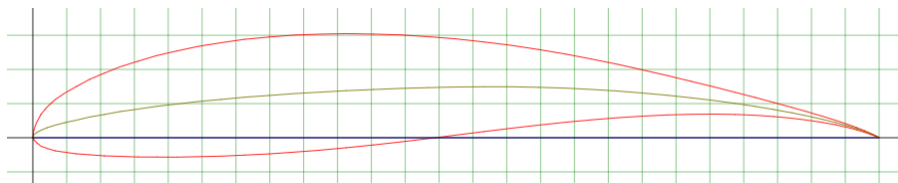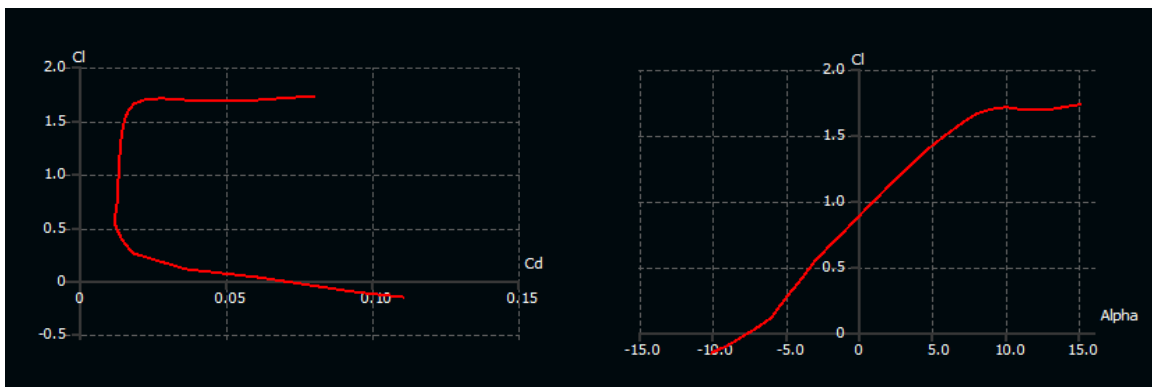

Figure 20: Profile of Wortmann FX-63 137B Airfoil

Figure 21: The variation of lift with drag coefficient (left) & angle of attack (right)
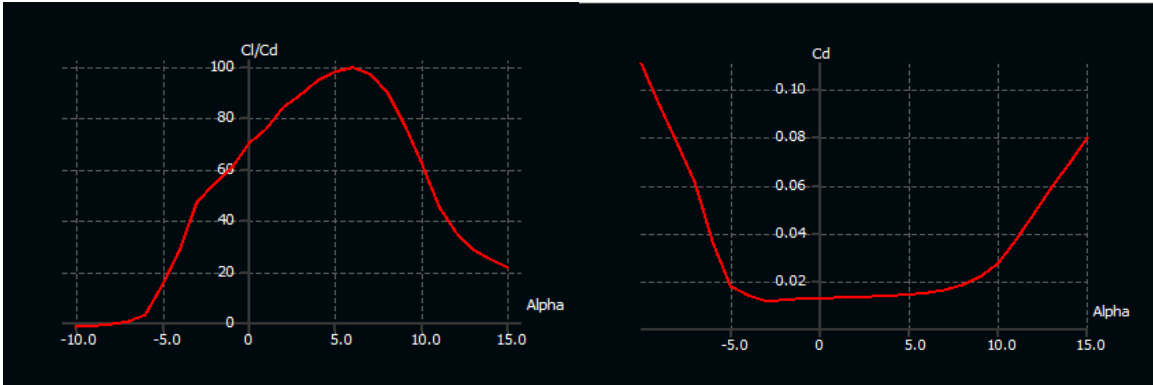
Figure 22: The variation of lift-to-drag ratio (left) & drag coefficient (right) with the angle of attack
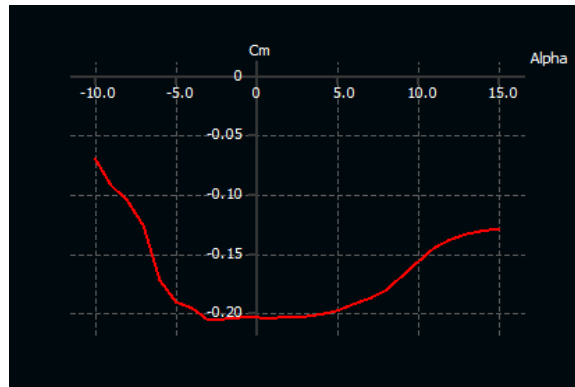
Figure 23: Variation of pitch moment coefficient with the angle of attack

Wing Design

The value of the taper ratio and incidence angle is selected iteratively, by determining the lift distribution over the wing using the lifting line theory and selecting the value which provides the best (elliptical) distribution. Open-source software XFLR iss used for this iterative process, which in addition to the lifting line theory, can also utilize the Vortex Lattice and 3D Panel Methods.

The airfoil's coordinates from *UIUC Airfoil Coordinates Database* are imported into the XFLR software and the finalized wing perimeters (wingspan and mean aerodynamic chord) inserted to define a wing. The studies are done at a low Reynold's number of 250 000 (laminar flow, less than 300 000), corresponding to a fixed wind speed of 16 m/s.
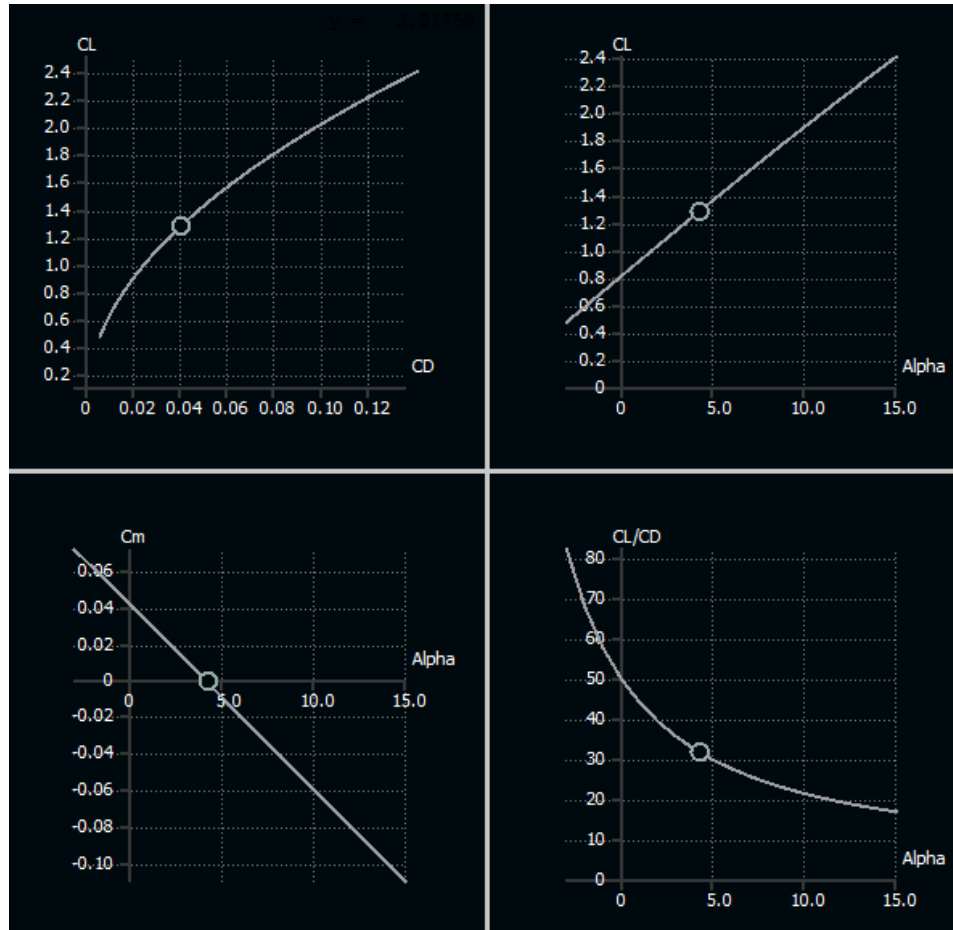
Figure 24: The variation of different aerodynamic parameters with the angle of attack for the wing

With the wing and boundary conditions defined, certain wing parameters, such as taper ratio and incidence angle are changed iteratively until the best lift distribution (elliptical) is obtained, alongside highest lift to drag ratio. Furthermore, the variation of lift, drag and pitching moment coefficients with angle of attack from -3 to 15 degrees is also noted and incorporated into the finalization of wing parameters. These graphs are shown in the figure below.

The changes in the geometry and their effects on the lift and drag are shown in **Appendix 1**. From this iterative process, the optimum value of taper ratio is found to be 0.6, with an incidence angle of zero.

Since the plane's span allows it to be quite stable on its own, no dihedral angle is set. To make the manufacturing process more straightforward, the twist angle is also set at zero.

The wing constitutes of two parts: a straight region (67 percent of total span) and a 0.6 tapered region (33 percent of total span). These values, supplemented by the MAC of 24.2 centimeters, give a root chord of 25 centimeters and tip chord of 20 centimeters.
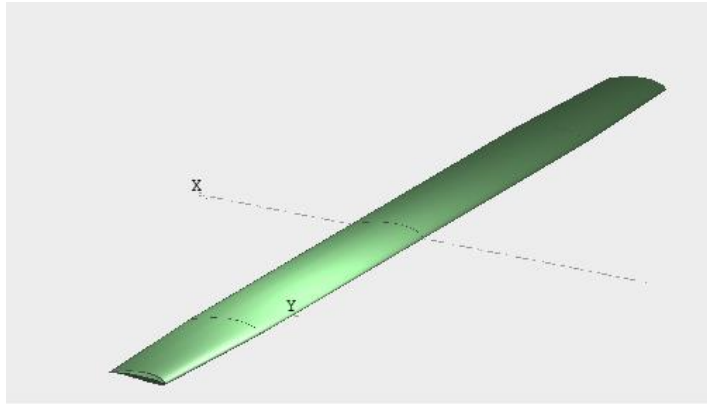

Figure 25: Defining Wing in XFLR

Tail Design

To make the design more straightforward and manufacturing easier, the conventional tail design is used for the sailplane. It must be noted however, that the conventional tail's horizontal component suffers from the flow distribution caused by the wing (since it is immediately behind the wing) and is therefore less efficient.

Generally, tails' profiles are made from symmetric airfoils, which do not produce any lift at zero angle of attack. Therefore, these need to be placed at a certain incidence angle which is determined based on the pitch stability of the airplane. The pitch moment and drag for the tail are usually neglected due to their very small values. The airfoil selected for the tail is NACA 0009, which is the most common symmetric airfoil used for tail design.

An essential parameter which links tail dimensions, such as its planform area S_h and position from the wing's leading-edge l, with wing area S and MAC is the tail volume coefficient, which is given by the following equation:

$$\overline{V}_H = \frac{l}{\overline{C}} \frac{S_h}{S}$$

For a horizontal tail, the tail volume coefficient is around 0.6, using which in the above equation provides the values of horizontal tail planform area and tail arm as 0.1 m² and 1 meter, respectively.

Similarly, for the vertical tail, the volume coefficient for a conventional tail is usually 0.03, and from this, the value of vertical tail area appears to be 0.07 m².

The tail's geometrical parameters, such as its span, chord, and taper ratio, etc, do not heavily influence the pitching moment. As such, they can be selected based on the already existent models of sailplanes, particularly the scale models. Based on the available data, the values of these parameters are listed below. For the sake of simplicity and easier manufacturing, no twist or dihedral angles have been incorporated.

- Horizontal Tail

  o Tail Area = S_h = 0.1 m^2
  o Tail Taper Ratio = λ_h = 0.6
  o Tail Root Chord = 17 cm
  o Tail Span = 75 cm
  o Tail AR = 5.512
- Vertical Tail

  o Tail Area = S_v = 0.07 m^2
  o Tail Taper Ratio = λ_v = 0.4
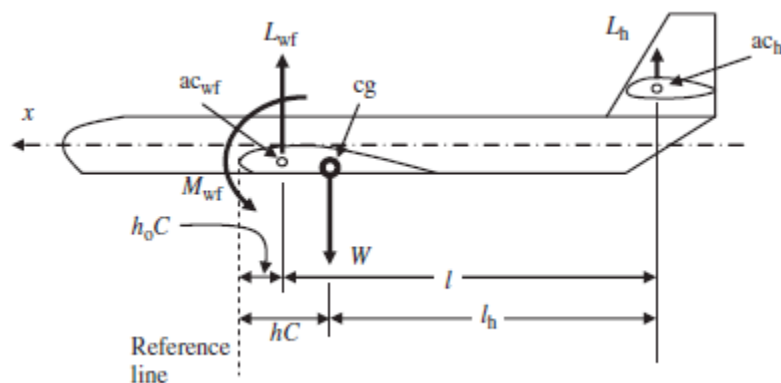 o Tail Root Chord = 28 cm
  o Tail Span = 35 cm

Figure 26: Free Body Diagram of the cruising plane

The incidence angle of the tail is determined by applying the pitch balancing conditions on the plane. The horizontal tail applies a thrust, usually negative (that is, downwards) to

balance the pitching moment produced by the wings. The balancing condition is achieved when the following static equilibrium equation, as derived from the free body diagram above, is satisfied:

$$C_{m_{0\_wf}} + C_L \left(h - h_o\right) - \eta_h \overline{V}_H C_{L_h} = 0$$

The above equation incorporates the locations of plane's center of gravity and its neutral point. For context, neutral point is the location where the plane's pitching moment becomes constant irrespective of the angle of attack. As such, the plane reverts to trim condition when disturbed. For the plane to be statically stable, the center of gravity must be ahead of the neutral point.

Furthermore, the pitching moment must decrease with the angle of attack, the rate of which is controlled by the position of center of gravity. The pitching moment value at an angle of attack is adjusted via the incidence angle of the tail.

Determining the location of neutral point is possible, albeit difficult analytically, and therefore, XFLR is used again for this purpose. With a setting angle of zero and inserting the tail parameters into the software, the pitching moment of the plane with the angle of attack is noted. The location of different modules and components of the sailplane is modeled in the software via point masses, and the plane's inertia is defined. Following this, the center of gravity of the plane is manipulated until the graph of pitching moment vs angle of attack becomes a straight line. This location of Center of gravity corresponds to the neutral point and is found to be 26 cm behind the wing's leading edge.

The extent of plane's static stability, and in essence the CG's distance from the neutral point, is expressed numerical as static margin, and is equal to the distance between them per MAC. Generally, a static margin of 13 percent is adequate, and using this value, the desired position of CG appears to be 23.6 cm behind the wing's leading edge.
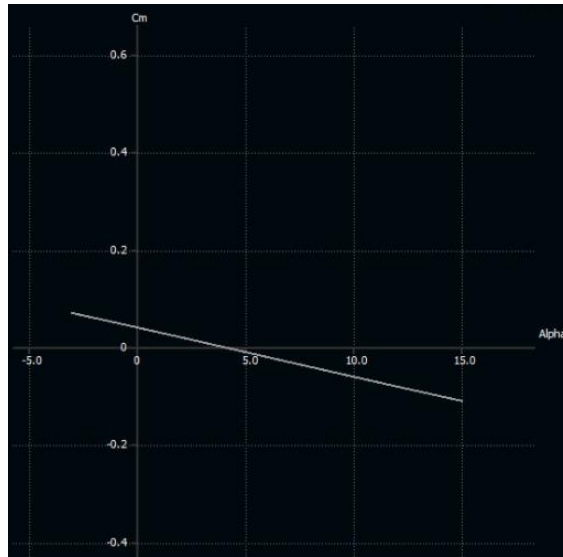
Figure 27: Plane Pitching moment coefficient variation with angle of attack

The zero AOA pitching moment with this static margin is at 0.5. This value must be positive, and slightly above the zero. For this purpose, the tail incidence angle is changed, until the desired results are obtained at an incidence angle of 4.5 degrees. The vertical tail's incidence angle remains zero since the plane is already stable along transversal axis.

Prototype Design

The sailplane is going to be made from balsa wood, which is a lightweight and sufficiently strong material commonly used for producing scale plane models. To reduce the weight, the entire model is made hollow, with inner ribs, braces, and truss-like structures for supports. For a CAD model, individual parts were designed and assembled in SolidWorks, majorly consisting of components such as fuselage, wings, and tail. The placement of different ribs/braces, and their thicknesses were selected based on different sailplane models of similar sizes made from balsa wood, such as Merylin 40A (4 meters span) and Blackhawk 7B (3.5 meters span). The complete model of the sailplane, indicated various ribs and braces, is illustrated in the figure below. The drawings of individual components can be found in Appendix.
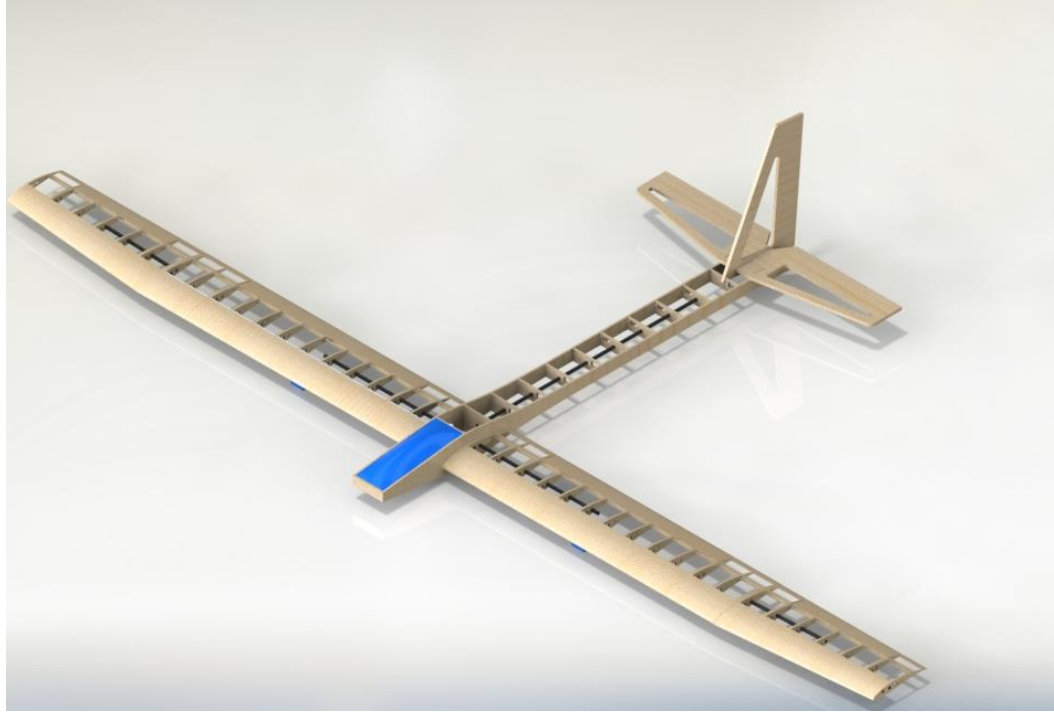
Figure 28: Rendered CAD Model of the Sailplane

Manufacturing Process

Entering the manufacturing phase, we started off by creating the structural skeleton of the plane later to be followed by software and controller integration. The steps were as follows:

Balsa Wood

Planks or slabs of Balsa wood were purchased that were sized as 1000mm x 100mm. These planks were off the thickness 10m m, 8mm, 6mm, 4mm, 3mm, and 2mm which were to be utilized for different parts of the plane as shown below.

The planks of these sizes were relatively small for the existing size of our aircraft and hence inter sheet bonds were required to be made at certain points as well which were planned in the design phase.
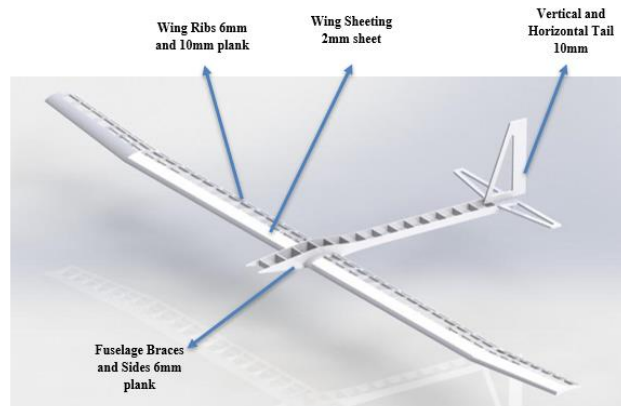
Figure 29: Sheet thicknesses at different parts of the sail plane.

Laser Cutting

To shape the planks and accurately cut them into parts that could be bought together to constitute structural parts of the plane, the planks of balsa wood need to accurately cut with laser cutting machine. The machine needs to be set at a wattage so that the laser beam is not strong enough to burn it, but it is strong enough of cut the part along the shape that has been fed into it through the DXF file.

Figure 30: Balsa Planks

Figure 31: Laser Cutting of 10mm Plank for Wing Rib

Figure 32: Finished Laser Cut Rib

Assembly of Laser Cut Parts

After approximately 200+ laser cut parts were produced from Balsa planks, the next step was to combine these parts to produce their requisite structural body. This was to be done with extreme care considering that the laser cut part had very minute tolerance amongst their sizes and the fitted very well on to each other however the bonding material to be used was to acquire a certain mass and volume as well.

Figure 33: Bonding Agent

The bonding agent that was used was an industrial grade epoxy by Bob Smith Industries with strength greater than 4500 psi. The parts bonded together with extreme care so as to ensure that no part is bonded eccentrically of at an angle. The affect of small mistakes that were made during tye process of manufacturing were evidently observed in the later stage where the assembly of different structural units became difficult. This was

overcome by sanding out the redundant or interfering parts. The parts were structurally bonded together in the following bodies:

1. Each rib of the wing was kept parallel to each other and a spar was used to bond them together from either side. This was, each wing was manufactured in two parts, the straight part and the tapered part which were eventually bonded together.

2. The two parrallel sheets of the Fuselage were bonded together via the braces. The complete fuselage was manufactured in two parts this was which were then bonded together in to a complete structure.

3. The tail was made through 10mm thickness parts that were sanded in order for them to acquire a smooth airfoil shape. These were then bonded together into a vertical and horizontal tail which fit into each other via a slip running across the vertical tail

Figure 34: Wing Assembly

Figure 35: Completed Wing Assembly

Figure 36: Tail and Fuselage

Structural Integrity via Carbon Tubes

To allow better bending resistance in the wings and Fuselage, 2 mm thick carbon fiber tubes with outer diameter of 10 mm were added in the ribs as well as in the joint between the straight and tapered part and the fuselage. Two of such rods that were extending out of the Fuselage were used to mount the wings. This made the wings modular and allowed for lesser logistical issue instead of having to mount the wings and transport the whole plane.

Figure 37: Carbon Fiber Rod in Fuselage

Control Surfaces

All these control surfaces were made by integral pieces of Balsa wood which were sanded to acquire a shape that would be suitable for such integration. Through were

incorporated through 1 cm deep hinges that were pushed into a slot made in the wing and flaps. As a result, an approximated 50-degree rotation was achieved on either side.

Figure 38: Flaps with Hinges on Wing

Mechanical Movement through Servos

The flaps are to be moved at certain controlled degree of angles through servo motors. We used 9g servo motors with approximately 2 kg torque for all the horizontal moving flaps while the rudder is controlled by a 15g 3.5 kg torque servo motor which were fitted by making a slot in the wood wherever necessary. Each servo was connected to an arm or lever which was connected to a push rod. This push rod made its way to a golden crown that was mounted on horn and this horn was screwed onto the flap.

In this was the circular rotation of the motor shaft translated into upward and downward rotation of the flap which is the desired output. A picture of the lever-push rod-crown-horn apparatus is shown below:

Figure 39: The lever-push rod-crown-horn apparatus

BLDC Motors and Clamps

The BLDC Motors were to be clamped onto either of the wings order to allow for thrust to drive the whole plane. The Clamping part was 3D Printed with PETG and was attached to the wings via a slot that made it was through to the carbon fiber rod of the wing for strength. This was done for both wings and the motor were then screwed onto the clamp. The propellers were then mounted on via a washer and nut as shown.

Figure 40: BLDC Mount with Propeller

Nose and Cockpit

Both cockpit and nose were 3D Printed and the cockpit was attached via a hinge to allow for it's opening during the flight gaps to change or fix wiring etc. The nose was also 3D printed with PLA and fixed to the front.
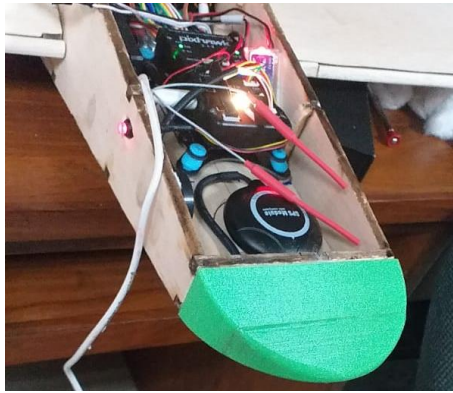

Figure 41: Nose

Solar Foil Sheeting

After complete wiring and structural integration as well as control calibration of the sail plane, the whole of the aircraft was sheeted in a Solar Foil which is a smooth sheet aerodynamically designed to allow smooth and streamlined air flow. The solar foil has a heat-based adhesive at it's one end. It was kept on the surface of balsa and heated via a heat gun or cloth iron to make it stick. The wrinkles were removed via further ironing or using a hair dryer. As a result, the surface the structural integration of aircraft was complete.

Figure 42: Solar Foil sheeted tail

Landing Gear

Landing gear made up of alloyed steel rods were used with nylon rubber tires. The total height of the front landing gear is approximately 13 cm which is enough to give requisite clearance to the sail plane propeller during takeoff.
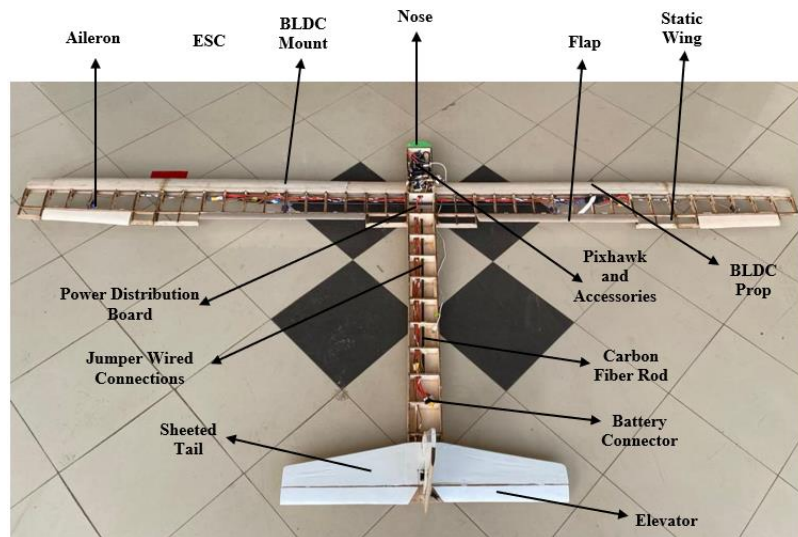

Figure 43: Labelled Unsheeted Sailplane

Avionics and Circuitry

After completing the mechanical portion of the assembly, we moved on to the setup of avionics, figuring out the circuitry and calibration of different software and hardware, used for the flight.

Servo Calibration

This stage was commenced by installing servo motors on our wings, and horizontal and vertical tail using the pushrod, horns, and screws. All specifications regarding servos are listed in Appendix A.3.

Next, connections of all the servos were extended to a point slightly before the nose of the fuselage using several jumper wires. This point is where our flight controller Pixhawk 2.4.8 will be installed. The connections of the jumper wire were clamped using the wiring tape.

Electronic Speed Controller Calibration

The next step was mounting, soldering, and extending the connections of ESCs to the fuselage. There were two ESCs we used for both of our wings. The one mounted on the left wing (as seen from the plane's rear) was rated 100A, whereas the one mounted on the right wing was rated 60A. Both were mounted near the throttling motors. Male and female bullet connectors of diameter 3mm were soldered to the output leads of the motor to the ESC on both wings.
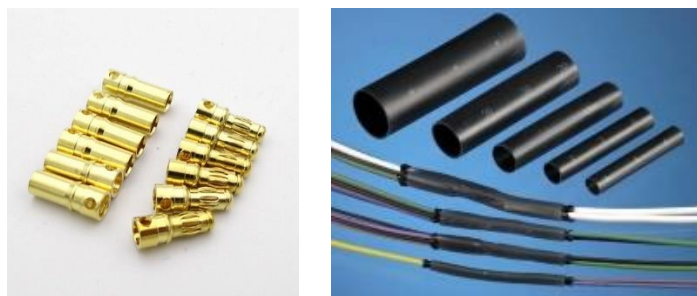

Figure 44: Bullet Connectors and Heat shrinks

The motor and ESC output leads were connected using bullet connectors. Next, the leads of the ESC which will be connected to the battery were extended to the fuselage using a pair of 12 AWG wires of length 0.55m for each wing. Lastly, the PWM leads (having a connector at their end) were also extended to the fuselage using several jumper wires. The connections between the jumper wires were clamped using wiring tape.

One XT60 (where 60 means 60A current rating) connector was soldered on the extension wire to attach the input leads of ESC to the extension wire. Heat shrinks were placed on the wire before soldering, and using a heat gun, were shrunk radially onto the soldered end of the wire.
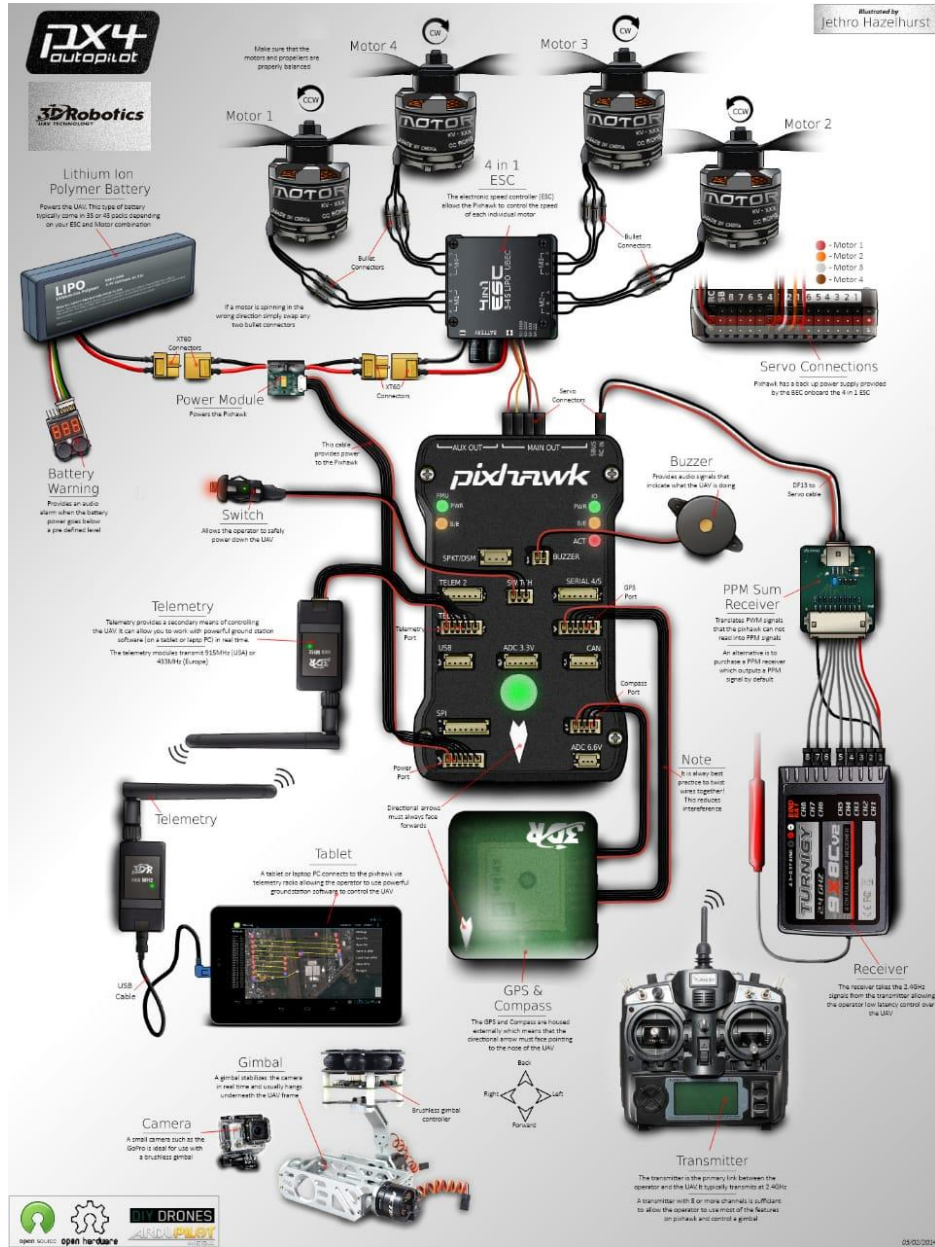
Circuit Diagram

Figure 45: Circuit Diagram

Flight controller

Because of its low cost, low weight, supplier availability, redundant sensors, wide I/O ports, and CPU performance, the Pixhawk 2.4.8 was chosen as the primary flight controller (see Figure below). This was flashed with firmware FMUv3 which served as the foundation for the real-time system identification work given here.

The Pixhawk is a 32-bit ARM Cortex M4 processor with a floating-point unit (FPU) for doing difficult arithmetic calculations. It has a 32-bit 24 MHz ARM Cortex M3 fail-safe co-processor and operates at 180 MHz with 256 KB of RAM. It features a Spectrum DSM/DSM2/DSM-X satellite receiver input port as well as a variety of other connectors (I2C, SPI, CAN, and USB). It has a 3-axis magnetometer and barometer, as well as two 16-bit IMUs for redundancy.

Figure 46: Flight Controller

GPS Module

We used the latest Ublox Neo-M8N GPS module, which contains a digital compass from QMC5883L. The ceramic patch antenna incorporates active electronics, and this module has a high level of sensitivity. It also comes with a protective plastic cover to keep it safe from the weather. This module contains a rechargeable backup battery for warm starts and produces precise location updates at 10Hz. The Ublox NEO-M8N is pre-configured

to work with Pixhawk and APM at a baud rate of 38400. The most significant benefit of this module is the high level of sensitivity it provides.

Figure 47: GPS Module

Power module

The APM 2.5 Power Module is a simple 6-pos connection that provides clean power from a LiPo battery as well as current usage and battery voltage readings to your APM 2.5. From up to an 8S LiPo battery, the onboard switching regulator delivers 5.3V and a maximum of 3A.
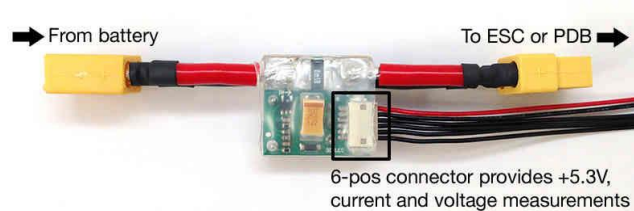

Figure 48: Power module of Pixhawk

Power Distribution Board

PDB (Power Distribution Board) is a board that allows distribution of electricity from the battery to the ESCs / Motors and create multiple voltage levels of power for the flight controller and other peripherals. PDB also can measure battery voltage and current. PDB simplifies and improves the reliability of high-power line connections.

Figure 49: Power Distribution Board being soldered

Radio Receiver

A radio receiver receives the radio signals and transforms them into some useful information or output. We used Flysky iA 10B 10CH Receiver. The transmitter it fits includes FS-I4 FS-I6 GT2E GT2G FS-I10 FS-I6S TH9X FS-CT6B GT3C CT3C FS-I4 FS-IT4S. The multi-axis aircraft model is compatible with the 10-channel receiver data return receiver remote control model. Only modules beginning with the letter C are allowed to be transferred in the interface.

Figure 50: FLysky iA 10B 10CH Radio Receiver

Radio Transmitter

A radio transmitter controller is used to allow the radio waves to be emitted. We used Flysky FS-16X 10CH 2.4Ghz RC Transmitter Controller for the project. The bandwidth of this system is between 2.408GHz and 2.475GHz. There are 135 channels in all. To avoid interference from other transmitters, each emitter bounces between 16 channels (32 for the Japanese and Korean versions).

Figure 51: FS-16X 10CH 2.4Ghz RC Transmitter Controller

Battery

Batteries are used to power the power module of the Pixhawk. We used MANIA X Power 3300 mAh LiPo Battery. The battery selection is primarily based on its capacity, measured in mAh, which is the number of milli-amperes it can continuously provide for an hour before discharging. Other selection criteria involve voltages and number of cells required by brushless motors and other equipment.

The brushless DC motors selected, Dongxingwei C3542, run on a voltage of 11.1 volts, and draw a maximum current of 48 Amperes each. The battery capacity is reflected in terms of the plane's flight time. Setting the flight time at 5 minutes at 100 percent throttle (quite unrealistic and conservative estimate, this much throttle is only required at takeoff), and given that fact the maximum drawn current is 96 Amperes, the required mAh come out to be 6500 mAh. To allow easier mobility and distributed weight, two 3300 mAh LiPo batteries were selected for the model.

Figure 52: Battery

Battery Eliminator Circuit (BEC)

A battery eliminator circuit (BEC) is an electronic voltage regulator used in battery-powered equipment to supply a subsystem at a different voltage without the usage of a supplemental battery. It is used to power the unpowered servo rail of the Pixhawk 2.4.8 (AUX IN rail). BEC is designed to drop the higher voltage to a lower magnitude of voltage. We used Hobbywing 3A UBEC, which is a switch-mode DC-DC regulator that comes with a lithium battery pack (or a NiMh/NiCd battery pack with 5-18 cells).

Figure 53: 3A-BEC

Pixhawk shock absorber

The Pixhawk 2.4.8 Universal Shock Absorber vibration dampening mount contains a central supporting plate that reduces vibration and is suitable for sensitive gadgets and cameras.

Figure 54: Pixhawk 2.4.8 Shock Absorber

Buzzer and Safety Switch

The passive buzzer and the Flight Controller E-Switch are normally included in the Pixhawk package. On one side of the Passive buzzer is a JST-SH connection that

connects directly to the Pixhawk. You'll be able to hear distinct noises which correspond to different modes once you're connected. The Pixhawk Flight Controller E-Switch Module allows quick arming and deactivation your board. A three-position JST-SH connection is included.

Figure 55: Buzzer and Safety Switch

Setting up Pixhawk and Avionics

Keeping in mind the circuit diagram shown above, insert all the leads and wires into their respective slots. As we are flying a plane, so servo leads can be inserted in any of the 1-8 Main Pins or the Aux 1-4 pins of the Pixhawk. BEC rail was inserted into AUX 6. The other 2 leads (power and ground), along with the 2 ESCs were soldered into the power distribution board (PDB). The power module was connected to the battery, PDB, and Pixhawk.

The radio receiver was inserted into the RCIN rail of the Pixhawk. Buzzer, GPS Module, and Safety Switch were inserted into the Pixhawk. Once, all these connections are done, we mounted GPS and Pixhawk (which is mounted on the shock absorber) onto the fuselage using the double-sided tape. We ensured that the GPS pointer and Pixhawk pointer are parallel and pointing toward the nose of the aircraft. We also ensured, that there is no bending induced in Pixhawk after mounting. The wiring diagram is also shown below to further elaborate.
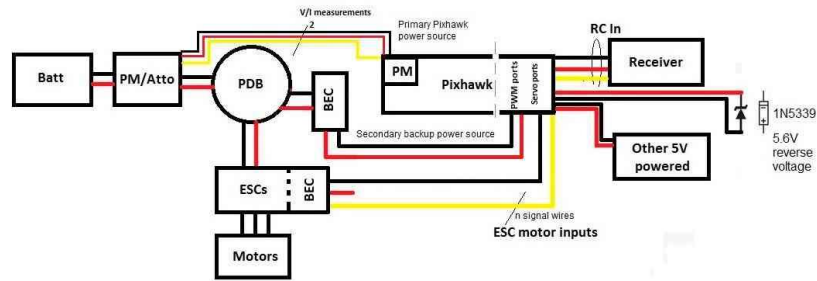
Figure 56: Wiring Diagram

Setting up and Calibration

The software used is called Mission planner which is downloaded from the Ardupilot website. Mission Planner was chosen because it is a sophisticated open-source tool with real-time waypoint navigation capabilities. The SITL simulator also includes a mission planner for testing rotor emulation techniques. We connected the Pixhawk hardware to the laptop i.e., the Mission planner using a Micro-USB cable. The Mission planner interface is shown below.

Then firmware FMUv3 is flashed for the Plane and the accelerometer is calibrated by keeping the plane level, nose-up, nose-down, back, front, left, and right. Then, we calibrate the compass by moving the plane randomly in 3D space.

Once it is done, we calibrated servo output by matching the function of the servo on the Mission planner with the corresponding rail on Pixhawk. After this, we calibrated the maximum and minimum position of all the servos, ensuring that all ailerons, flaps, rudders, and elevators were at 0°.

Next, we performed binding of the radio transmitter with the receiver. Then, we performed the radio calibration on the Mission planner for all channels 1-9 by moving sticks on the transmitter controller to their maximum and minimum. We ensured that we clicked reverse for ailerons as ailerons on each wing need to deviate in opposite direction to each other.

Next, we specified the function of the throttle by matching the rail on the Pixhawk for both motors. Ensure that the plane is armed using the safety switch to test servos and armed using both the safety switch and Arm button on Mission Planner to test the motor. We also ensured Failsafe is disarmed to test servos and motors.

Figure 57: Interface of Mission Planner

CHAPTER 4: RESULTS AND DISCUSSIONS

Computational Fluid Mechanics (CFD)

To compare our results with the data of Appendix 1, we simulated a model of wing using *FX 63-137B* inside a wind tunnel using Computational Fluid Dynamics (CFD) in *Ansys 2021 R2.* The analysis system opted for the analysis is *Fluent.*

We created the wing by importing the coordinates from the *.txt* file of the airfoil. We made a surface using the airfoil curve plotted and extruded it 2.345m symmetrically along the sketch plane on both sides, after scaling it.
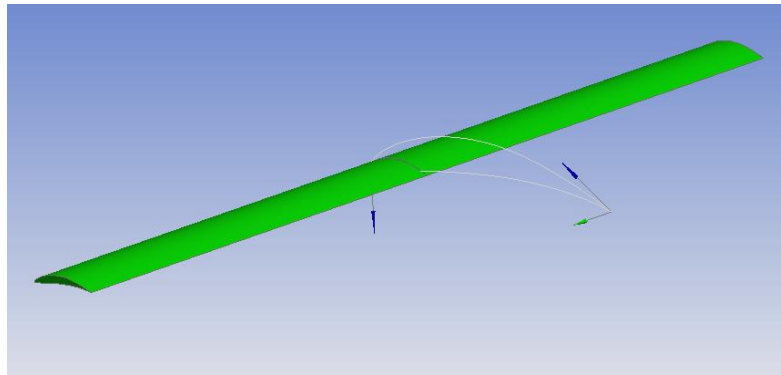

Figure 58: Wing Model in ANSYS Design Modeler

Next, we created an *enclosure* to model the wind tunnel and applied symmetry along the plane of symmetry of the enclosure to get the half wing. To perform analysis, we subtracted the wing from the enclosure. Now, we moved to the mechanical module of the *ANSYS Workbench,* where we performed the meshing of the model. Settings for the mesh were kept as follows:

- Element size of the enclosure: 0.5m
- Element size of the wing (after sizing command): 0.05m
- Growth rate: 1.1
- Elements: 404759
- Nodes: 80459

We also introduced *mesh inflation* around the wing. The settings were:

- Inflation option: *Total Thickness*
- Number of Layers: 10
- Growth Rate: 1.2
- Max. thickness: 0.008m

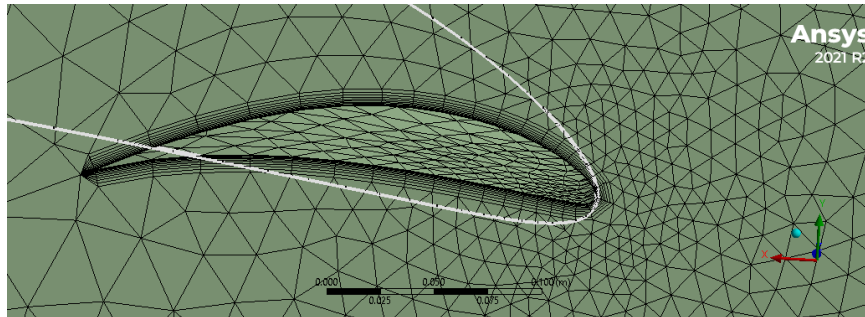A mesh was generated of the model, which is shown:
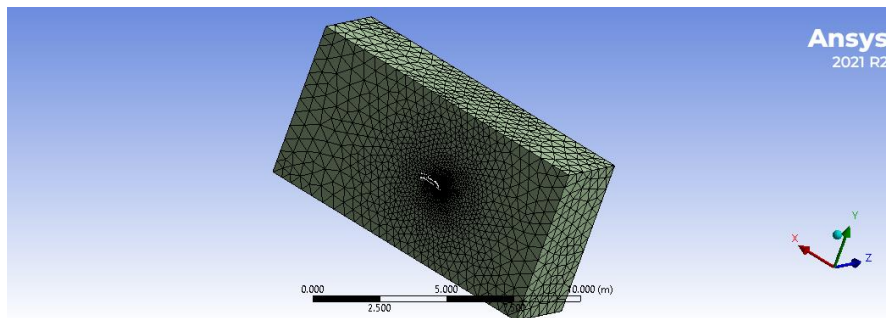

Figure 59: Mesh sequence of the Wing

Figure 60: Mesh sequence of the model

We updated the mesh sequence and moved onto the fluent module to compute the solution.

Choosing viscous model as *Spalart-Allmaras*, with velocity at inlet to be 18m/s as *boundary condition*, we initialized the system using our reference values as following:

- Density = 1.16 kg/m^3
- Viscosity = 1.8 e-05 Pa.s
- Area = 0.76 m^2

Finally, we computed our solution using *200 iterations,* generating lift and drag coefficients (Cl and Cd) on the wing in our report, which came out to be:

- **Cl: 0.67**
- **Cd: 0.023**

To check our lift coefficients and drag coefficients after the complete assembly, we performed Computational Fluid Dynamics (CFD) once again. We also plotted Streamlines, Downwash, Viscous Drag, Pressure Distribution, and Lift Distribution. The results are shown below:
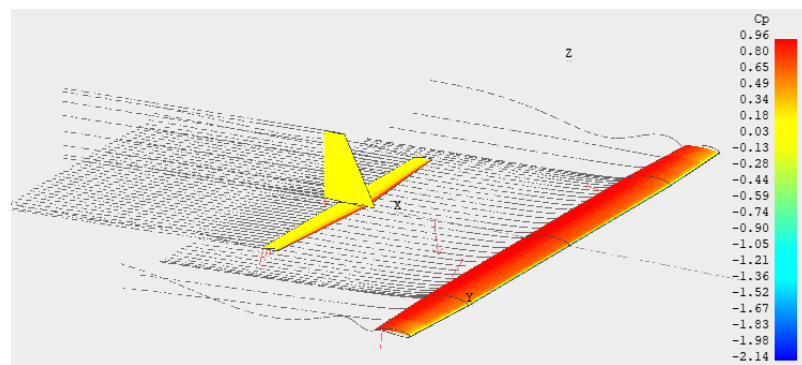

Figure 61: Coefficient of Pressure distribution over the plane surface
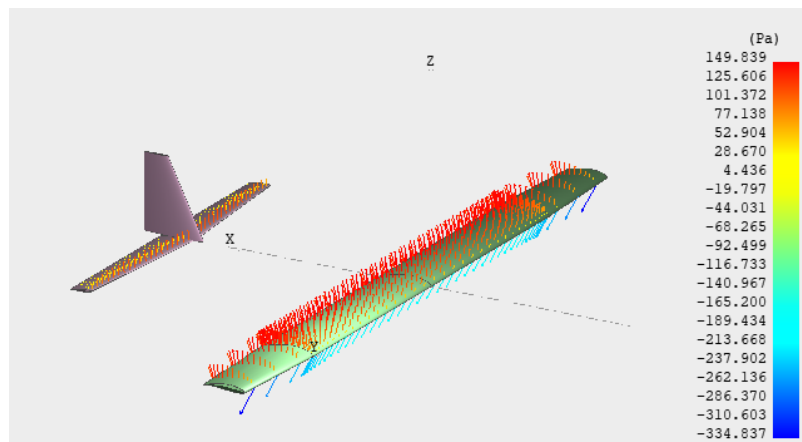

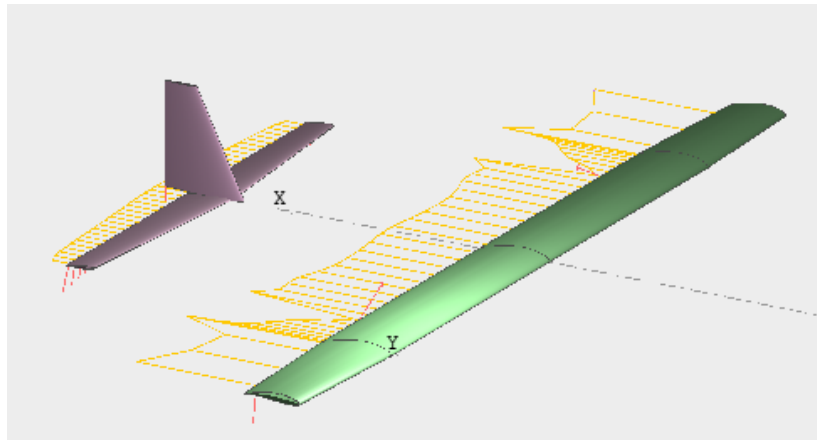**Figure 62:** Pressure distribution over the plane surface

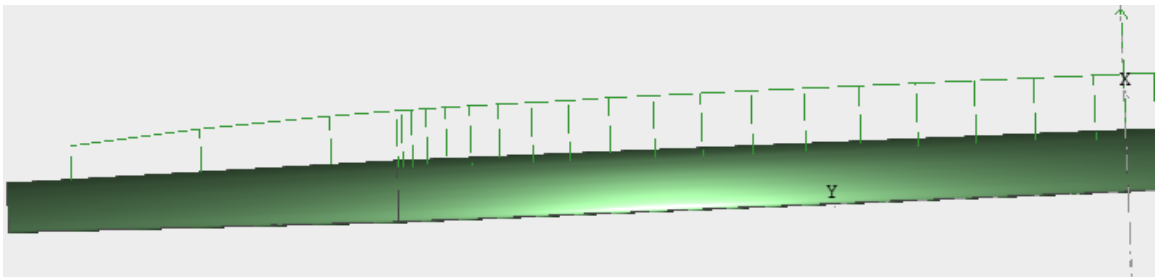**Figure 63:** Viscous Drag over the plane surface

Figure 64: Elliptical Lift Distribution on the wing
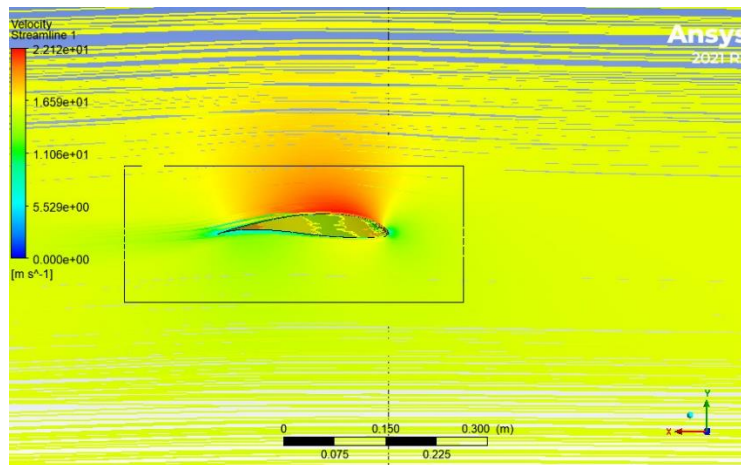

Figure 65: Flow streamlines over the wing, as approximated by CFD

A comparison of lift and drag coefficients provided by XFLR and Ansys CFD is given in the following table (Re = 250 000):

Parameter	XFLR	ANSYS
Lift Coefficient	0.816	0.67
Drag Coefficient	0.016	0.023
Glide Ratio (Cl/Cd)	50	29.1

Therefore, we observe that there is a difference in the values of the coefficients produced in both software. One of the reasons is the fact that XFLR does not incorporate viscous models while producing coefficients, whereas ANSYS incorporates different viscous models for each type of flow. XFLR produces an approximate solution whereas ANSYS uses various models, boundary conditions, and equations to produce a solution.

Testing

The test flight was planned in the SNS ground road in mildly diffused sunlight at around 5PM with mild wind speed of approximately 24km/ or 6m/s. The expected outcomes of the practical test flight are as follows:

1. The ground must be chosen to be a road or cemented pavement considering that the plane acquires the speed of approximately 3 to 4 meters per second due to the propeller thrust which can be further increased by giving artificial thrust (via a tether tied to a vehicle etc.)
2. The span of the plane's wing requires at least 6 meters of space on the road due to the vortices of wind formed at the outer edges of the wing. Therefore, the complete road needs to be cordoned off.
3. The plane's ailerons do not play any role in elevating the plane to the height during take-off. The flaps and elevators need incremental angle as the plane is about to take off while the ailerons stay in their neutral position.
4. The plane's yaw motion is entirely governed by the rudder however a small amount of angle change that was observed during the assembly of the tail on the fuselage may directly affect how well the plane is able to change its yaw motion. This eccentricity can also cause the plane to bank or show unwanted yaw during its flight which needs to be spontaneously balanced by the rudder motion.
5. The plane's roll motion is entirely governed by the ailerons and the motion of the ailerons is always counter to that of each other since they are calibrated in that manner.

6. Each of the flap, elevator, aileron, or rudder is allowed a motion of at least 30 degrees from its neutral position mechanically as well as electrically.

7. The Flaps must be made through integral parts considering that they need to sustain a certain amount of incoming inertia of wing. The idea of making the flaps with less mass and slits in not adequate and was given up after the realization that those flaps are very prone to breaking.

CHAPTER 5: CONCLUSION AND RECOMMENDATION

Pakistan is not self-sufficient in its energy needs. The high cost of a wind powerplant, specifically the Windmills, generally keeps investors and the government away from wind power and hence our wind power sector; entirely unexploited. We need a cheap and efficient method to harvest wind energy. The only exploited avenue for wind energy in Pakistan are windmills which involve high structural and machinery cost. The current solution provides much cheaper & efficient solution to access higher winds with the expertise, technology, equipment, and material indigenously available. Within Pakistan, no registered company employs the same solution to harvest high wind energy. International companies producing on-board generation system notably include Makani Power and Ampyx Power. We intend to introduce same technology in Pakistan to meet clean and renewable energy needs.

Therefore, using our analysis and calculations, we conclude that our sailplane (rigid wing) will have a mass of 15 kgs, with a wingspan of 4.69m. The aspect ratio will be 20, with the planform area equal to 1.1m2. The airfoil opted for the sailplane is CH10-48-13, with taper ratio coming out to be 1.0, i.e., a rectangular planform. There will be no incidence angle or sweep angle for our wing. The sailplane will be flying up to an altitude of 100m, where it will cruise at a speed of 18m/s. The software used for analysis i.e., XFLR and ANSYS, gave us an idea of the real-life environment at 100m altitude, which served as a helping hand in shortlisting values for different parameters needed for the construction of the sailplane.

REFRENCES

- 2022. [online] Available at: <https://www.researchgate.net/publication/282314959_Airborne_Wind_Energy_Systems_A_review_of_the_technologies/figures?lo=1> [Accessed 30 January 2022].
- Peter Harrop. Biomimetic aircraft snatch power aloft, October 2012
- Skywindpower.com. 2022. Sky Windpower. [online] Available at: <https://www.skywindpower.com/> [Accessed 30 January 2022].
- Engineering.purdue.edu. 2022. [online] Available at: <https://engineering.purdue.edu/~aerodyn/AAE333/FALL10/HOMEWORKS/HW13/XFLR5_v6.01_Beta_Win32%282%29/Release/Guidelines.pdf> [Accessed 30 January 2022].
- M-selig.ae.illinois.edu. 2022. UIUC Airfoil Data Site. [online] Available at: <https://m-selig.ae.illinois.edu/ads/coord_database.html> [Accessed 30 January 2022]
- Usgs.gov. 2022. What materials are used to make wind turbines? | U.S. Geological Survey. [online] Available at: <https://www.usgs.gov/faqs/what-materials-are-used-make-wind-turbines#:~:text=According%20to%20a%20report%20from,aluminum%20(0-2%25).> [Accessed 30 January 2022].
- Tutiempo Network, S., 2022. Climate Islamabad Airport (February 2018) - Climate data (415710). [online] www.tutiempo.net. Available at: <https://en.tutiempo.net/climate/02-2018/ws-415710.html> [Accessed 30 January 2022].
- Tutiempo Network, S., 2022. Climate Islamabad Airport (February 2018) - Climate data (415710). [online] www.tutiempo.net. Available at: <https://en.tutiempo.net/climate/02-2018/ws-415710.html> [Accessed 30 January 2022].
- 2022. [online] Available at: <https://www.smarthobby.pk/product-page/pixhawk-2-4-8-gps-ublox-m8n-power-module-set> [Accessed 29 May 2022].
- 2022. [online] Available at: <https://www.smarthobby.pk/product-page/pixhawk-2-4-8-gps-ublox-m8n-power-module-set> [Accessed 29 May 2022].
- 2022. [online] Available at: <https://www.smarthobby.pk/product-page/pixhawk-2-4-8-gps-ublox-m8n-power-module-set> [Accessed 29 May 2022].
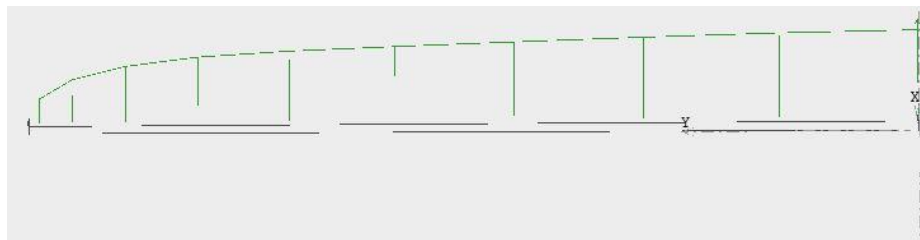
APPENDICES

Appendix I: Results of XFLR Wing Analysis

- Half wingspan = 2.345m, Area = 1.1m^2, Tip chord = Root Chord = 0.2345m, Taper Ratio = 1, Aspect Ratio = 20, Angle of Attack = 0 deg
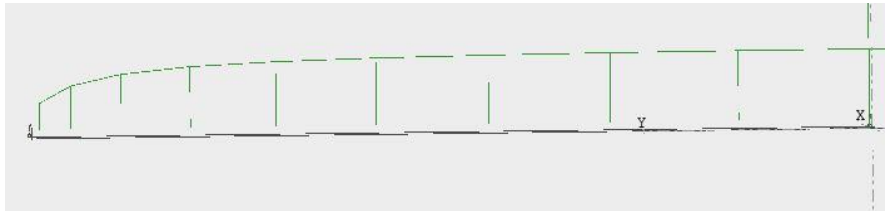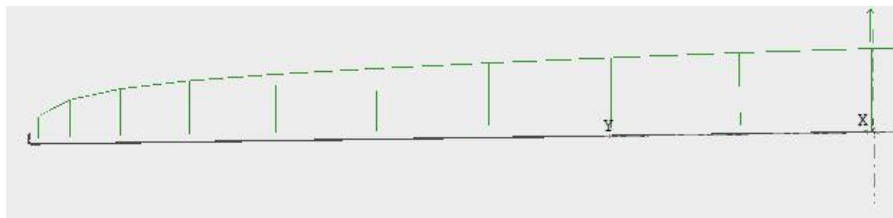

Cd = 0.044, Cl = 0.949, Cl/Cd = 21.361

- Half wingspan = 2.000m, Area = 0.72m^2, Tip chord = 0.160m, Root Chord = 0.200m, Taper Ratio = 0.8, Aspect Ratio = 22.2, Angle of Attack = 0 deg
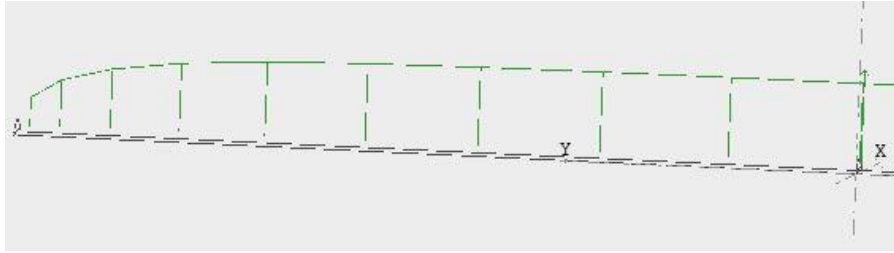

Cd = 0.048, Cl = 0.870, Cl/Cd = 18.187

- Half wingspan = 2.345m, Area = 0.99m^2, Tip chord = 0.187m, Root Chord = 0.2345m, Taper Ratio = 0.8, Aspect Ratio = 22.3, Angle of Attack = 0 deg
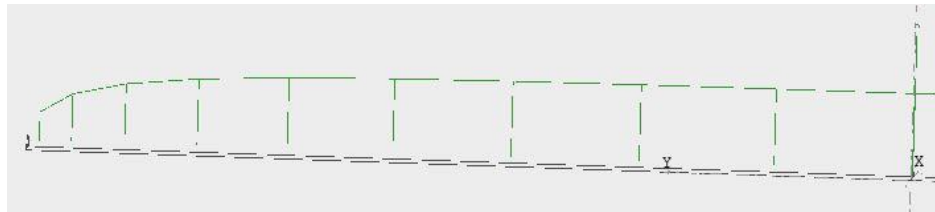

Cd = 0.045, Cl = 0.925, Cl/Cd = 20.748

- Half wingspan = 1.870m, Area = 0.70m^2, Tip chord = Root Chord = 0.187m, Taper Ratio = 1, Aspect Ratio = 20, Angle of Attack = 0 deg

Cd = 0.050, Cl = 0.856, Cl/Cd = 17.211

- Half wingspan = 2.345m, Area = 1.1m^2, Tip chord = Root Chord = 0.2345m, Taper Ratio = 1, Aspect Ratio = 20, Angle of Attack = 0 deg

Cd = 0.047 Cl = 0.985, Cl/Cd = 21.007

- Half wingspan = 2.000m, Area = 0.72m^2, Tip chord = 0.160m, Root Chord = 0.200m, Taper Ratio = 0.8, Aspect Ratio = 22.2, Angle of Attack = 0 deg

Appendix II: MATLAB Code for Preliminary Analysis

```matlab
syms WS_Vs(V_s) WP_Vmax(WS) WP_S_TO(WS) WP_ROC(WS) WP_AC(WS)
```

Design Parameters

```matlab
m = 150/9.81;          % Total mass (kg)
Vs = 10;          % Stall Speed (m/s)
V_max = 21.7;     % Maximum Speed (m/s)
S_TO = 20     ;   % Take off distance (m)
ROC = 1.3        ;   % Rate of climb (m/s)
h = 100          ; % Operational Height (m)
h_AC = 150        ;% Absolute Ceiling (m)
```

Assumed Parameters

```matlab
AR = 20;          % Wing Aspect Ratio
mu = 0.04;        % Runway friction coeff
C_Lmax = 2.2;     % Max. Lift Coeff
C_D_o = 0.015 %0.014;   % Zero-lift drag coeff.
LD_max = 20;      % Max. Lift to Drag Ratio
eta_p = 0.7;       % Propellor Efficiency
eta_p_c = 0.55; % Propellor Eff. at takeoff
```

Constants

```matlab
rho_o = alt_density(0);     % kg/m^3
rho = alt_density(h)   ;     % kg/m^3
rho_AC = alt_density(h_AC); % kg/m^3
g = 9.81;                     % m/s^2
sigma = rho/rho_o;
sigma_AC = rho_AC/rho_o;
W=m*g;
e = 0.8;
K = 1/(pi*e*AR);
V_TO = 1.2*Vs; % Take-off speed
C_D_oLG = 0.012;
C_D_oHLDTO = 0.008;
C_D_oTO = C_D_o + C_D_oLG + C_D_oHLDTO;
C_L_C = 0.3; % 0.3 for sub-sonic aircraft
C_L_flapTO = 0.5; % Usually 0.3-0.8
C_L_TO = C_L_C + C_L_flapTO; % Take-off lift
```

```matlab
C_D_TO = C_D_oTO + K*C_L_TO^2; % Take-off drag

C_D_G = C_D_TO - (mu*C_L_TO);

C_L_R = C_Lmax/(1.2^2);
```

Stall Speed

```matlab
str2sym("(1/2)*rho*C_Lmax*(V_s^2)")

WS_Vs(V_s) = (1/2)*rho*C_Lmax*(V_s^2);

vpa(WS_Vs(Vs),4)
```

Maximum Speed

```matlab
str2sym("eta_p /
((0.5*rho_o*(V_max^3)*C_D_o*(1/WS))+(2*K*(1/rho)*(1/sigma)*(1/V_max)*WS))")

WP_Vmax(WS) = vpa(eta_p /
((0.5*rho_o*(V_max^3)*C_D_o*(1/WS))+(2*K*(1/rho)*(1/sigma)*(1/V_max)*WS)))
```

Take off Run

```matlab
str2sym("(1-(exp(0.6*rho*g*C_D_G*S_TO*(1/WS))))/(mu-
((mu+(C_D_G/C_L_R))*(exp(0.6*rho*g*C_D_G*S_TO*(1/WS)))))*(eta_p/V_TO)")

WP_S_TO(WS) = vpa((1-(exp(0.6*rho*g*C_D_G*S_TO*(1/WS))))/(mu-
((mu+(C_D_G/C_L_R))*(exp(0.6*rho*g*C_D_G*S_TO*(1/WS)))))*(eta_p/V_TO))
```

Rate of Climb

```matlab
str2sym("(1/((ROC/eta_p_c)+(1.155/(LD_max*eta_p_c))*sqrt((2/rho)*sqrt(K/(3*C_D_o))*WS))
)")

WP_ROC(WS) =
vpa(1/((ROC/eta_p_c)+(1.155/(LD_max*eta_p_c))*sqrt((2/rho)*sqrt(K/(3*C_D_o))*WS))
```

Absolute Ceiling

```matlab
str2sym("(sigma_AC/((1.155/(LD_max*eta_p_c))*sqrt((2/rho_AC)*sqrt(K/(3*C_D_o))*WS)))")

WP_AC(WS) =
vpa(sigma_AC/((1.155/(LD_max*eta_p_c))*sqrt((2/rho_AC)*sqrt(K/(3*C_D_o))*WS)))
```

Appendix III: Dimensions & Specifications of Electronic Components

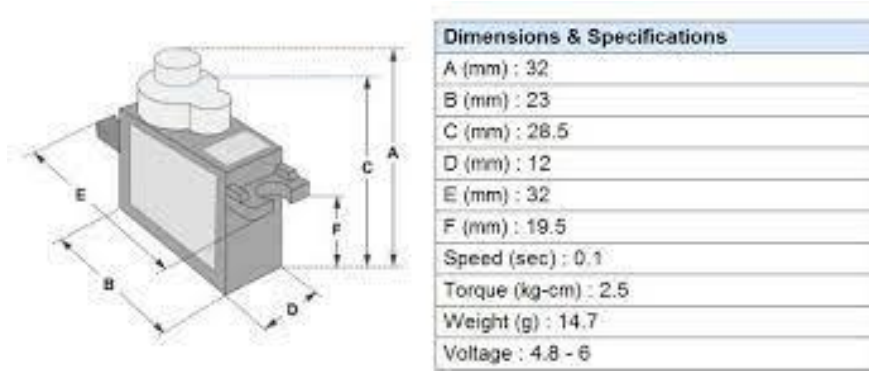**Figure 66:** BLDC Specifications and drawing

Figure 67: Dimensions and specifications of 9g servo motor

Technical specifications:
- Voltage: 11,1V
- Capacity: 3300mAh
- Discharge rate: 35C (115,5A)
- Discharge rate Peak: 70C (231,0A)
- Charging current: 1-3C Max 5C
- Dimensions H*W*L : 21*44*138mm
- Weight: 258 g
- Balancer connector: XH
- Discharge cable length: 14cm
- Discharge cable: 12AWG
- Discharge connector: XT60

Figure 68: MANIA X LiPo Battery Specifications